NTNU – Trondheim
Norwegian University of
Science and Technology

Drivers of the high frequency variability of gravity wave forcing in the mesosphere and lower thermosphere

Hanne Synnøve Pettersen
Linde

Master of Science in Physics and Mathematics
Submission date: June 2015
Supervisor: Robert Edward Hibbins, IFY

Norwegian University of Science and Technology
Department of Physics

Acknowledgements

I would like to thank my supervisor professor Robert Hibbins for his excellent guidance throughout my work. Also a thanks goes to Nora Stray for assisting me when downloading the MERRA data.

Abstract

In this thesis the influence of gravity waves (GWs) in the mesosphere/lower thermosphere (MLT) was analysed. This was inspired by the work done in the paper by de Wit et al. (2014), which used the SKiYMET meteor radar in Trondheim (63.4°N, 10.4°E) to study the seasonal cycle of the GW forcing (GWF) in the MLT, in 2013. The results agreed well with previous research, but a high temporal frequency variability in the GWF was also observed that could not be explained any further. The intention for this thesis was therefore to investigate possible mechanisms that could cause this variability. This was done by studying the atmosphere below the MLT on a daily basis, with the focus on GW generation and activity. Information about the wind speed in the atmosphere, which was used to measure the GWs, was obtained by meteorological reanalysis.

The three mechanisms studied were the GW generation in the troposphere, described by the tropospheric winds, secondly, the GW activity in the lower stratosphere, which was derived from the kinetic energy of the GWs and thirdly, the GW filtering which measured the atmospheric transmission of GWs from the ground to the MLT. Finally, the variability in each part was compared to the variability in the GWF. The results revealed correlation coefficients that varied between -0.2958 to 0.6932, significantly correlated above the 99% confidence level. Investigations were undertaken to determine if these correlations were due primarily to the seasonal cycle of the GWF. When the seasonal effects were removed through filtering, all of the correlation coefficients dropped and became insignificant. Hence, neither of these mechanisms could explain the high frequency variability in the GWF in more detail. On the other hand, it was found that by applying a restriction on the phase speed of the GWs that propagated through the GW filter, slightly improved the correlation with the GWF on a seasonal basis. Compared to no restriction, it went from explaining 42% to 48% of the variance in the GWF. This was an interesting result which could be investigated further to see if it could be implemented in weather and climate models to take account for the GW effect more accurately.

Sammendrag

Denne masteroppgaven har sett på hvordan gravitasjonsbølger har påvirket mesosfæren og nedre del av termosfæren (engelsk: MLT). Inspirert av artikkelen til de Wit et al. (2014) hvor det ble brukt en SKiYMET meteorradar i Trondheim (63.4°N, 10.4°E) til å studere hvordan gravitasjonsbølger påvirket MLT, kalt GWF (engelsk: gravity wave forcing), i løpet av 2013. Resultatene deres stemte godt overens med tidligere forskning, men en høyfrekvent vertikal variabilitet i GWF ble også observert som ikke kunne forklares. Målet med denne oppgaven var dermed å undersøke ulike mekanismer som kunne forårsake denne variabiliteten. Dette ble gjort ved å studere atmosfæren nedenfor MLT daglig, med fokuset på gravitasjonsbølgenes opprinnelse og bevegelse. Informasjon om vindhastigheten i atmosfæren som ble brukt til å beskrive gravitasjonsbølgene, kom fra reanalyser av meteorologiske data.

De tre mekanismene som ble studert var gravitasjonsbølgenes opprinnelse i troposfæren, beskrevet av vindhastigheten i troposfæren, deretter, gravitasjonsbølgenes bevegelser i nedre del av stratosfæren, som var utledet fra gravitasjonsbølgenes kinetiske energi, og til sist filtreringen av gravitasjonsbølger som var et mål på den atmosfæriske transmisjonen av gravitasjonsbølger fra bakkenivå og opp til MLT. Til slutt ble variabiliteten i hver del sammenlignet med variabiliteten i GWF. Resultatene viste korrelasjonskoeffisienter mellom -0.2958 og 0.6932, signifikant på minst et 99% konfidensnivå. Undersøkelser ble deretter utført for å se om korrelasjonene var primært et resultat av årstidene. Da effektene av årstidene ble filtrert bort, sank korrelasjonskoeffisientene og var ikke lenger signifikante. Dermed kunne ingen av disse mekanismene forklare den høyfrekvente variabiliteten i GWF i større detalj. På en annen side ble det funnet at ved å sette en restriksjon på hastigheten til gravitasjonsbølgene som beveget seg gjennom gravitasjonsbølgefilteret, økte korrelasjonen med GWF på en årlig basis. Sammenlignet med ingen restriksjon gikk den fra å forklare 42% til 48% av årstidstrendene i GWF. Dette var et interessant resultat som kan bli undersøkt videre for å finne ut om det er mulig å implementere dette i vær- og klimamodeller slik at effekten av gravitasjonsbølger kan bli målt mer nøyaktig.

Table of Contents

List of Tables

List of Figures

Abbreviations

GCM	=	Global circulation model
GPS	=	Global positioning system
GW	=	Gravity wave
GWF	=	Gravity wave forcing
hPa	=	Hectopascal (unit)
IR	=	Infrared
KE	=	Kinetic energy
mb	=	Millibar (unit)
MERRA	=	Modern-era retrospective analysis for research and applications
MLT	=	Mesosphere/lower thermosphere
NASA	=	National aeronautics and space administration
NH	=	Northern hemisphere
PW	=	Planetary wave
SH	=	Southern hemisphere
SKiYMET	=	All-sky interferometric meteor radar
SSW	=	Sudden stratospheric warming
UTC	=	Coordinated universal time
UV	=	Ultra violet

Chapter 1

Introduction

One thing that most people have in common is an opinion about the weather. Knowing what the current state is and how it will change is of great interest, as it impacts many aspects of our lives. However, predicting the weather is not easy. A typical example is the numerous weather forecasts which have promised sunshine when rain suddenly arrives. This illustrates the difficulty to determine how parameters like the wind speed, the amount of clouds, precipitation and so on, interfere with weather. These are examples of chaotic variables that can change rapidly, and which impact the weather on small temporal and spatial scales. With this in mind, studies on the atmosphere are indeed important. Not just to be able to understand how the different mechanisms are connected with each other, but also to understand how it works as a whole. To have the knowledge about how the atmosphere behaves both on small and large scale is essential to make better weather and climate models. With good models the weather can be predicted more accurately, and more precise results can be achieved from climate studies. After all, the models only get as good as the physics included in them.

This master thesis was motivated by the work done in the paper by de Wit et al. (2014). Here a feature of the atmosphere called gravity waves (GWs) was studied in more detail. GWs are small atmospheric waves on a global scale which are generated in the lower parts of the atmosphere. The restoring force driving these waves is gravity, hence the name. Atmospheric waves can be compared to waves in the ocean, both important for the transport of energy and momentum over various distances. GWs propagate vertically and at higher altitudes they will break and deposit their momentum. Hence, they couple the atmosphere by influencing the atmospheric circulation at these altitudes. This impact will in turn affect both the weather and the climate. Moreover, GWs are believed to be the main driver of the mesosphere/lower thermosphere (MLT) region, which is situated about 90 km above ground. GWs have been observed for a long time, but it is only recently that their influences in the higher parts of the atmosphere have been recognised (eg. Holton, 1983; Fritts and Alexander, 2003). Therefore, by studying theses waves and their impact in the MLT, weather and climate models can be improved by including their effects in the higher parts of the atmosphere as well (Hocking, 2001).

The study by de Wit et al. (2014) was based on data from Trondheim (63.4°N, 10.4°E) in 2013. The results showed that GWs played a crucial role regarding transportation of energy and momentum from the lower parts of the atmosphere to the higher parts. There was found a clear relationship between the stratospheric wind variability and the gravity wave forcing (GWF) in the MLT. This was in good accordance with earlier research. However, the measurements of

the GWF had some unexplained high frequency variability as well. Therefore, the aim for this master thesis was to look into this variability in more detail, focusing on the GW generation and activity below the MLT on a daily basis. On this background the topic for this thesis became:

Drivers of the high frequency variability of gravity wave forcing in the mesosphere and lower thermosphere.

GW generation and activity can be studied by looking at wind speed variations in the atmosphere. The wind speed will provide a measure on the strength of these waves. Information about this was had from reanalysis data from a climate model and radiosondes (the device attached to weather balloons). The first gave information about the wind speed in the troposphere (lower atmosphere), and the zonal (eastward/westward) wind speed in the middle atmosphere. The latter about the kinetic energy per unit mass of the GWs in the lower stratosphere (middle atmosphere). The intention was to see if the variability in any of these different parts was correlated to the high frequency variability observed in the GWF. And hence, could explain this variability in more detail. Finally, the analysis was split into three questions:

1. Does the **tropospheric wind variability**, which is a measure of GW source variability, affect the GWF?
2. Does the **GW activity in the lower stratosphere** or more specifically, the kinetic energy per unit mass of the GWs affect the GWF?
3. Do atmospheric winds between the ground and 80 km affect the GWF by influencing the amount of GWs reaching the MLT, also known as **GW filtering**?

Chapter 2

Background

2.1 Basic atmospheric physics

The atmosphere can roughly be divided into vertical layers based on how temperature changes with altitude (Andrews, 2005). Figure 2.1 shows an illustration of this. One thing to notice is that the altitude is often given in hectopascals (hPa), which measures the pressure, instead of the distance to ground. The axis to the right in the figure is given in millibars (mb), where 1 mb equals 1 hPa, and the left one is given in km. Further, the temperature is related to the balance between the radiative, convective and dynamical heating/cooling processes in the atmosphere (Ramaswamy, 2006). The lower part, called the troposphere, goes from 0-15 km in altitude, and this is where most weather occurs. The middle part goes from 15-90 km and includes the stratosphere and the mesosphere. On top lies the upper part, called the thermosphere that goes all the way into space. Moreover, the region including the mesosphere and the lower parts of the thermosphere is commonly known as the MLT.

Further, the height of the layers is not constant and will have some variations, which follows the seasons and the underlying topography. Also, the boundaries between each layer are not well defined, and will merge due to the atmosphere being a continuous mix of interacting molecules. The density in each layer varies a lot as well. In fact, 90% of the atmospheric mass (i.e. molecules of different kinds) is found in the troposphere, 10% in the stratosphere and only 0.1% in the mesosphere and above (Andrews, 2005). Even though the density is extremely low in the higher parts, they still play an important role when studying the atmosphere as a whole.

The heat from the Sun is distributed horizontally and vertically according to the chemical and physical properties of the atmospheric molecules. The main properties in the different layers mentioned above, can briefly be described as the following. First, in the *troposhere* when air moves up and away from the ground, which is warm and acts as a heating source, the temperature will decrease. The rate of the decrease is affected by the state of the weather, geography and moisture (Ramaswamy, 2006). Further, in the *stratosphere* the increase of temperature with altitude ends in a temperature maximum in the stratopause. This is a result from O_2 and O_3 (oxygen and ozone) absorbing the UV-radiation that has not already been stopped by the atmosphere higher up (Plane, 2003). It is actually the UV-absorption by ozone that is the reason for the heating in the stratosphere (Holton, 2004). Moreover, the ozone layer is found here as well. This layer blocks UV-rays from going further down and potentially harming life. Then, in

the *mesosphere* the temperature starts to decrease again. The pressure here is very low, so the UV-radiation reaching the mesosphere will not be absorbed. Also, the CO_2 (carbon dioxide) present will contribute to more cooling by radiating local IR-waves (Plane, 2003). As a result, the coldest place in the atmosphere is found in the mesopause. Lastly, the increase of temperature in the *thermosphere* is caused by the absorption of the incoming short wave UV- and X-ray radiation, mainly by O_2 and N_2 (nitrogen). Due to the extremely low pressure in this region these temperatures are kinematic (Plane, 2003).

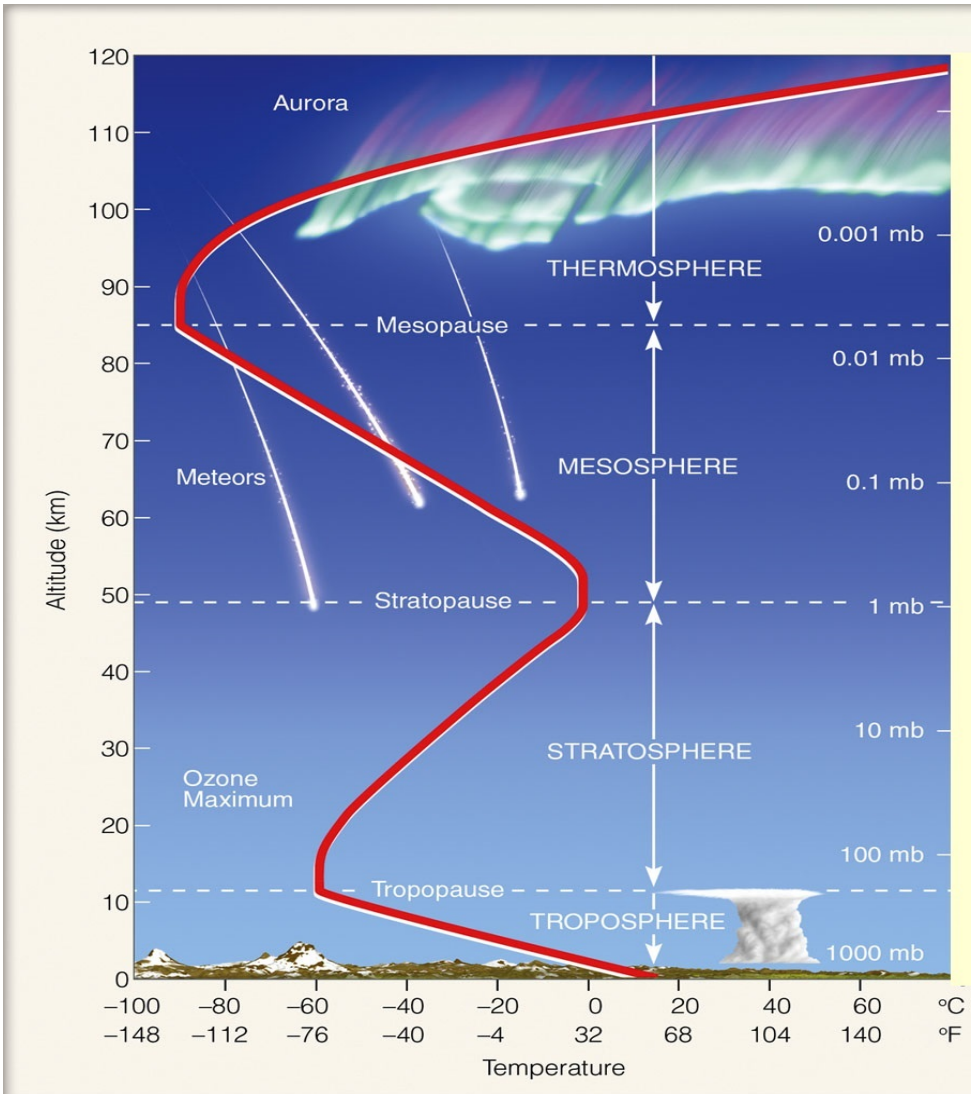

Figure 2.1: An illustration of how the atmosphere is divided into layers according to how the temperature (red line) changes (Hithcock, 2005).

The main energy source for the Earth-atmosphere system is the Sun. The radiative properties of this system (absorption, reflection and scattering) decide how the energy gets distributed. Figure 2.2 shows an informative illustration of the Earth's radiation budget. However, there will be deviations from this budget since parameters like the incoming solar radiation and the absorption/reflection are different at different locations. But an annual average will look more or less like this.

First look at the left side of the figure. Here the incoming short wave radiation from the Sun (yellow lines) hits the atmosphere. 19% gets absorbed by molecules and clouds, and 51% gets absorbed by the surface. The orange lines show how much of the radiation that will be reflected right back to space. This is on average 30% and is called the albedo of the Earth (Earth Observatory, 2014). The albedo is a number between 0-100% that tells how well an object reflects incident light. Different materials will have different albedos. For instance, ice has a high albedo of 84%, which means that 84% of the incident light gets reflected while 16% gets absorbed. The albedo of a green forest is only about 14% (Earth Observatory, 2014).

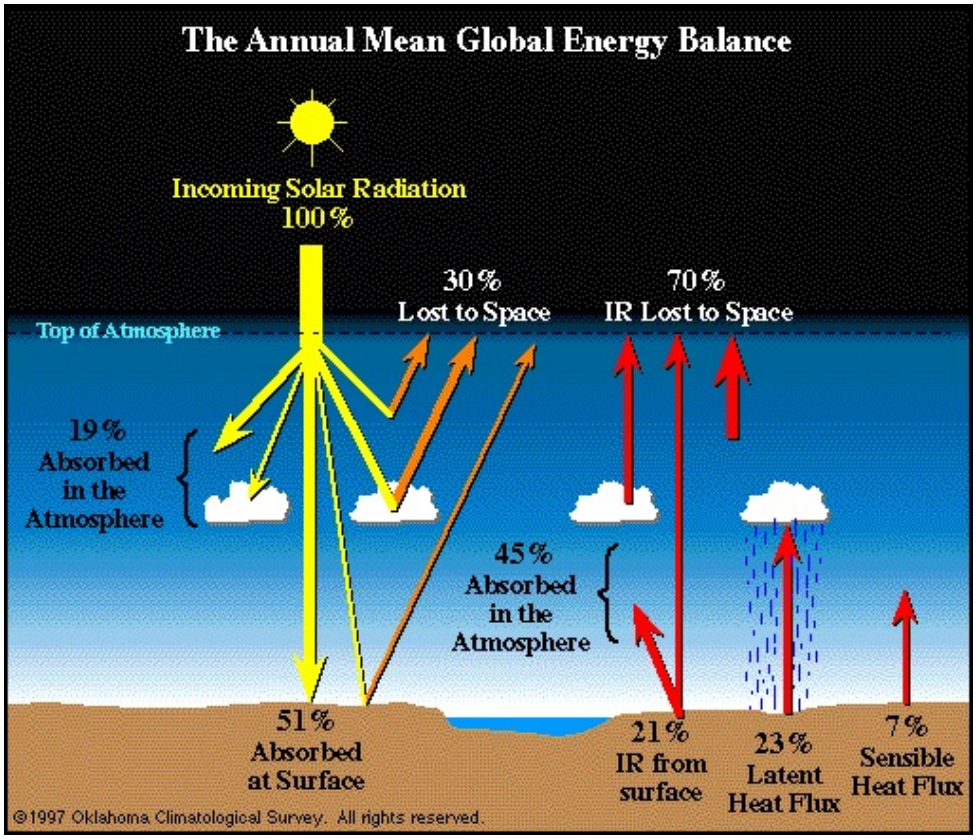

Figure 2.2: An illustration of how radiation from the Sun gets averagely distributed in the atmosphere (Oklahoma climatological survey, 1997).

Next, look on the right side of the figure. Of the 51% absorbed radiation from the Sun, the Earth's surface will re-emit the incoming short wave radiation, as long wave radiation in the IR-field, shown as red lines (Andrews, 2005). Of this long wave radiation 45% gets absorbed by the atmosphere, and will be re-emitted as heat. It is in fact this heat that warms the Earth; more commonly known as the 'greenhouse effect'. Furthermore, the molecules that contributes the most to this heating are called greenhouse gases, like CO_2 and water vapour. Without these the Earth's mean temperature would be -18°C and not 15°C (Ma, 1998). So the Earth actually heats from below.

Other heat related radiations from the Earth's surface are the latent heat flux and the sensible heat flux. The first is related to the phase change (solid, liquid or gas) of a substance. For example it is the heat required to melt ice into water, or the heat released to the surroundings when water vapour condenses into liquid water. The sensible heat flux is associated with the actual temperature of a substance (IPCC, 2014). Both play an important role in the Earth's energy

budget, mainly in the troposphere (Holton, 2004).

When looking at the atmosphere as a whole it can be viewed upon as a fluid of air covering the Earth. Therefore, research on atmospheric wave phenomena is of interest to understand, for example how energy is transported over various distances. In this thesis the variability of a type of wave found in the atmosphere called gravity waves, will be studied.

2.2 Gravity waves

Gravity waves (GWs) in the atmosphere are a type of oscillations caused by density differences in the air (Hocking, 2001). The restoring force driving these waves is gravity, hence the name, but they are also known as buoyancy waves[1]. GWs are found throughout the atmosphere and are important for the transport of energy and momentum (Andrews, 2005).

GWs are created when a parcel of air is displaced vertically. Since the density of the air decreases when going upwards, the density of the displaced air will be higher than the surrounding air. Gravity will then act on the denser air pulling it down. When descending, the parcel of air will at some point have less density than the air surrounding it. Then buoyancy will push the parcel upwards until areas of less density are reached, and the process repeats itself with gravity pulling the air downwards again. Hence, an oscillation has begun. To get a parcel of air to rise a displacement event must occur. Typically this happens when air flows over topography (orographic waves) e.g. the Scandinavian mountain range. In this case, some parts of the air will be pushed upwards and because of the density differences, gravity will pull it down again. They can also be created by convection for example in thunderstorms, or by unstable wind shear, wave-wave interaction and around fast moving wind streams to name some (Fritts and Alexander, 2003). However, not all of the mechanisms regarding GW generation are fully understood, and are still a field of active research (Fritts and Alexander, 2003). Further, GWs can be found inside a medium, like air or water, and will be called internal gravity waves. Or in the boundary layers between different mediums, for example air/water or water/oil. Common for all mediums is that the density must decrease with height and be stable, else gravity will not be able to restore the displaced air (Hocking, 2001).

To describe the physics behind GWs in more detail, figure 2.3 can be useful. Imagine a corrugated sheet being moved horizontally through a medium like air. This movement will displace some parts of the air upwards, and some parts of the air downwards. The air particles at point 'A' in the figure will be pushed up and forward by the corrugated sheet. This results in a velocity component 'w' upwards, and 'u' forwards. Thus, this air will move along the purple arrow. Since this air is pushed upwards its density will be accordingly higher. The grey area along the purple arrow indicates an area of higher pressure. At point 'B' the opposite will happen. Here the air will be pushed downwards and to the left, which will create an area of low pressure, shown by the thin grey lines. This repeats throughout the corrugated sheet. The orange dotted line beside the point 'D' in the figure can be disregarded as it is not used to describe the physics here.

[1]It is important to differ gravity waves from gravitational waves, the latter being theoretical perturbations of space-time (Stuver, 2013).

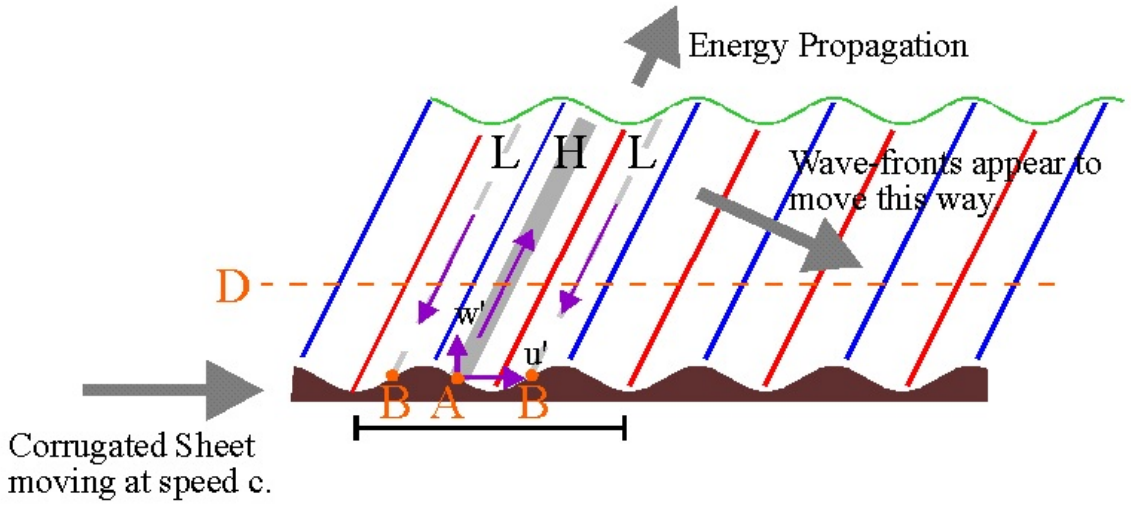

Figure 2.3: Visualising the physical properties of gravity waves with a corrugated sheet moving through a medium (Hocking, 2001).

The waves created will have a horizontal component, namely the grey arrow labelled 'wave fronts seems to move this way', and a vertical component, labelled 'energy propagation' in the figure. Furthermore, the horizontal wavelength can be 100-1000 km and is much larger than the vertical wavelength, which can be 100 m-20 km (Hocking, 2001). Since GWs are small waves on a global scale, the Coriolis force can be neglected (Andrews, 2005). Lastly, the blue and red lines indicates areas of lower and higher temperature caused by the air being moved up and down adiabatically.

It is the vertical component that has the greatest impact on the atmosphere. Conservation of energy will make the amplitudes of the waves larger as they propagate higher up, since the density decreases. When these waves reach areas of unstable conditions or where the background wind equals the horizontal phase speed, they will dissipate or break, and deposit their momentum. This momentum transfer from the lower atmosphere to the middle and upper atmosphere will influence the atmospheric circulation (Vincent, 2009). GWs can enhance or weaken this circulation as the friction force enforced is anti-parallel to the wind direction (Espy, 2015). With that said, GWs couple the atmosphere vertically and are believed to be the main driver of the circulation in the MLT (e.g. Holton, 1983; Lindzen, 1981).

When GWs and the higher parts of the atmosphere were included in weather and climate models, the output became more precise (Hocking, 2001). This illustrates the importance of the energy transfer, and hence the vertical atmospheric coupling done by GWs. However, since GWs are small scale waves, they are hard to resolve in large scale models like global circulation models (GCM). Research on how to take account for their influence on larger scales are therefore of great interest. Also, some of the dynamics and effects of GW generation and propagation are hard to quantify. This is due to the chaotic nature of interactions and coupling in the atmosphere. And some are not yet known. For instance, turbulence, reflection and refraction in the middle atmosphere caused by unstable winds, are dynamics that affect GWs and can modify further propagation (Fritts and Alexander, 2003). Hence, the results obtained from GW studies can be influenced by unknown effects in the middle atmosphere. More research is therefore needed to get the full picture of these waves. As a final mark, the movements of GWs can

sometimes be seen as ripples in the clouds, see figures 2.4 and 2.5. They can also be felt as turbulence by planes flying through these waves.

Figure 2.4: Traces of gravity wave movements over New Hampshire, Vermont (Gibson, 2014).

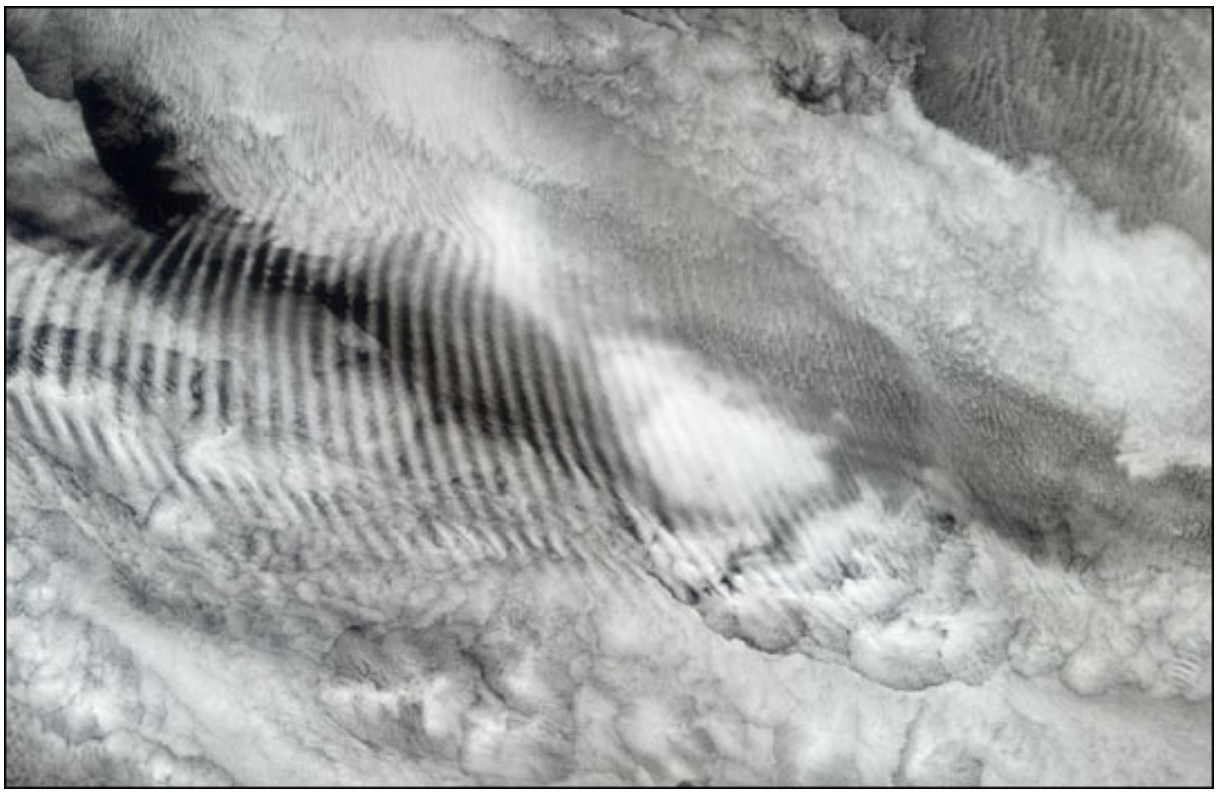

Figure 2.5: Gravity wave ripples over the Indian Ocean (Earth Observatory, 2004).

2.3 Stratospheric filtering

GWs couple the atmosphere vertically by transferring momentum to higher altitudes, with the strongest influence in the MLT. What portion of the GW spectrum that reaches the MLT region is actually decided by the atmospheric conditions in the stratosphere. The winds here namely change their direction according to winter and summer time (Andrews, 2005). In more detail, when the Northern Hemisphere (NH) has winter the stratospheric winds move eastwards and in summer they move westwards. This is because when the NH has winter the North Pole is turned away from the Sun, while the South Pole is turned towards the Sun. This leads to more warming at the South Pole, and less warming at the North Pole. Higher temperature means higher pressure in the air, and a pressure gradient going from high to low pressure (south to north) is established. This in turn will decide the wind direction going the same way. Hence, this meridional wind transports heat from the south and to the north (Whiteway et al., 1994). Because the Earth is rotating the Coriolis force acts on the wind direction as well. It deflects it to the left in the SH and to the right in the NH. That is why the NH stratosphere has eastward winds in winter and westward winds in summer. The same applies for the SH in winter and summer.

The direction of the stratospheric wind will affect the GWs. That is, when the NH has winter, GWs with an eastward phase speed will be stopped from propagating any further by the eastward winds in the stratosphere (Fritts and Alexander, 2003). This is because the phase speed is equal to the background wind. To put it another way, GWs with matching phase speed as the background wind will be absorbed. On the contrary, GWs with a westward phase speed will not be stopped and can propagate upwards. When these waves break the MLT will experience a westward GW forcing (GWF). In summer it is opposite, see figure 2.6 for details. Hence, the stratosphere works as a filter deciding which GWs and how much of these GWs are allowed to propagate upwards.

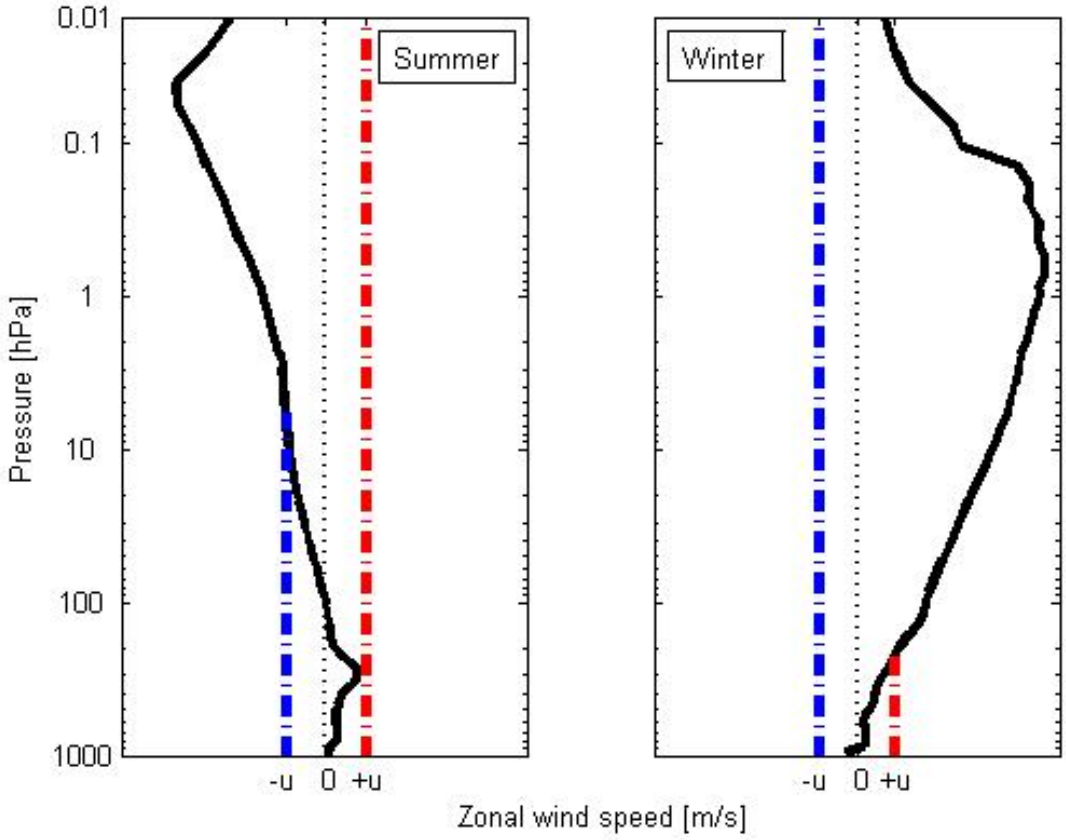

Figure 2.6: Typical wind profiles (black solid lines) for the summer and winter stratosphere. The blue lines indicate westward winds and the red lines indicate eastward winds. In summer, the wind profile blocks westward winds and allows eastward winds to propagate up to the MLT, and vice versa in winter. The plots are based on MERRA data from July and December in 2013 measured over Trondheim.

2.4 Sudden stratospheric warming

Sudden stratospheric warmings (SSWs) are stratospheric phenomena that take place in the winter season in high northern latitudes (Coy et al., 2013). Under these events the stratosphere experiences a rapid increase of temperature typically during a period of a few days. This is believed to be a result from an increased activity of planetary waves (PWs) influencing the stratospheric polar vortex (Holton, 2004). PWs are atmospheric westward propagating waves on a global scale. Land/ocean contrast can create these waves as the pressure will vary over these areas due to different thermal properties. That is why large SSWs are mostly happening in the NH where most of the Earth's landmass is located. Large SSWs, which alter the wind flow down to 30 hPa, seem to take place once in every two years (Holton, 2004). Besides, smaller SSWs can be observed in both hemispheres during winter times.

The stratosphere during winter is dominated by an eastward polar vortex (Mukhtarov et al., 2007). With a meridional flow going from equator to the winter pole, due to higher pressure at equator caused by more solar heating. From time to time PWs with a westward phase speed will propagate upwards, and deposit their momentum. This will weaken the strength of the vortex. This in turn allows even more PWs to reach the stratosphere. To stay in a radiative balance,

the meridional flow changes direction and adiabatically warms the stratosphere. A cooling in the mesosphere is also observed (Holton, 1983; Mukhtarov et al., 2007). As more weakening takes place the polar vortex can in the end turn westward. When this happens the PWs will be blocked since their phase speed now matches the background wind. Then the PWs will start to deposit their momentum below this blocking level. This leads to the blocking level moving downwards. In the end, with no more forcing from the PWs the stratosphere will go back to its normal condition with an eastward polar vortex.

The change in the stratospheric wind will have an effect on the stratospheric wind profile, and hence the filtering of GWs, as described in the previous section. When the stratospheric wind profile is eastward (westward), GWs with an eastward (westward) phase speed are blocked, and a westward (eastward) forcing is seen in the MLT. In early January 2013 a large SSW took place (Coy et al., 2013). An analysis of the GWF by de Wit et al. (2014) showed that the GWF changed from westward to eastward and back to westward again, following the SSW. Furthermore, a simulation run by Holton (1983) showed that GWs reaching the MLT under a SSW were strongly reduced. Other studies show similar results (e.g. Hoffmann et al., 2012; Whiteway et al., 1994). Lastly, the response from the stratosphere and the mesosphere under a SSW is not uniform at all longitudes, as de Wit et al. (2014) show with satellite observations. So the location of the observing system also plays a role.

2.5 Observing the atmosphere

To observe the atmosphere two approaches are commonly used; in-situ observation and remote sensing or sounding (Andrews, 2005). In-situ refers to methods where the data is acquired inside a system i.e. in physical contact with the variables. Examples can be a weather station observing the wind speed or a weather balloon measuring the humidity in the air it flows through. Remote sensing on the other hand is observation of variables from outside the system i.e. not in physical contact with the variables. Satellites orbiting the Earth observing the temperature or ground based radars measuring the precipitation are used for this.

Different methods have different qualities. In-situ measurements often have high resolution in a restricted area where the measuring instrument is placed. Remote sensing on the other hand can cover large areas but the resolution cannot be as good as in-situ observations. To get the best results a mixture of several methods should be used. This thesis uses data from three sources. First from the MERRA project (see description in the next section), which is a result from remote sensing and numerical models. Then the results from meteor radar measurements, which is described in section 2.7. And finally, data from radiosondes (the device attached to weather balloons), provided by the University of Wyoming (Department of Atmospheric Science, 2013). The radiosondes are of the type Vaisala RS80 and their movements are tracked by GPS (Siikamäki, 2004). The measurements from the radiosondes will provide a snapshot of the atmosphere, since it only takes a couple of hours before the weather balloons burst. Thus, this can be used to study variations in the atmosphere on small temporal scales. This coincide well with GW behaviour. Further, the weather balloons are launched twice a day from Ørlandet (63.7°N, 9.6°E), which is about 50 km northwest of Trondheim. Ørlandet is one out of six launching sites in Norway operated by the Norwegian Meteorological Institute. They are responsible for the launches and obtaining and distributing the data to the rest of the world (Norwegian Meteorological Institute, 2009).

2.6 MERRA data

The modern-era retrospective analysis for research and applications or MERRA, is a reanalysis project by the National Aeronautics and Space Administration (NASA). It combines observational data from satellites with numerical models to produce variables that are not easily observed (Global Modelling and Assimilation Office, 2012). These variables are mainly used to study the variability of the weather and the climate. Observational data has been gathered since 1979 and is available for download from their web page (Earth Data, 2014). The system used for the reanalysis is the Goddard Earth Observing System Model, version 5 (GEOS-5), with its Atmospheric Data Assimilation System (ADAS), version 5.2.0 (Lucchesi, 2012). For more information about the model and assimilation system see (Rienecker et al., 2008).

In the model the Earth's surface is divided into a grid structure with the best resolution of 1/2° latitude $\times$ 2/3° longitude (Global Modelling and Assimilation Office, 2012). In the vertical direction a data set with 72 levels is available. Ranging from 976 hPa to 0.015 hPa (Lucchesi, 2012, 'Appendix C'), which is ground level to about 80 km, just below the mesopause. This data set follows the terrain and will give a better output at ground level compared to other available data sets (Stray, 2015). The variables are observed/calculated on a six hour interval (Lucchesi, 2012, 'Appendix A'). For more information about the MERRA variables see (Lucchesi, 2012). This thesis will study the zonal and meridional wind, or the u and v component as they are named in MERRA. The values of these are measured from satellites, radiosondes, aircraft reports, ships and buoyancy observations to name some.

2.7 Previous studies on gravity wave effects in the middle and upper atmosphere

As mentioned in the introduction, this master thesis is motivated by the work done in the paper by de Wit et al. (2014). In more detail, this paper performed amongst other things, a data analysis of the high-frequency GW momentum flux. The high-frequency momentum flux gives a measure on the propagation direction as well as the strength of the GWs. This can further be used to study the impacts of the GWs in the MLT. This was done by using a SKiYMET meteor radar situated in Trondheim (63.4°N, 10.4°E) in 2013.

A meteor radar can be used to examine the atmosphere at high altitudes. When a meteor enters the atmosphere it will interact with air molecules and leave behind an ionised trail of particles (Singer et al., 2004). This trail is of interest since it will drift on the background wind present. By observing this trail, the state of the background atmosphere can be found. Meteoric parameters like the radial velocity, height, amplitude and decay time, and atmospheric parameters like the wind speed and temperature, can also be determined. Meteors typically burn up between 70-110 km (Hocking et al., 2001) with a peak at 90 km, which is about the height of the MLT. Moreover, the number of meteors follows a diurnal cycle with most detections in the early morning hours. Seasonal effects are also observed, with an increasing number of meteors around the equinoxes at high altitudes (de Wit et al., 2014). During a day between 7,000-12,000 meteors can be detected by the Trondheim SKiYMET radar. The limiting factor for the SKiYMET will be the temporal resolution, which is the number of meteors per unit time. This should be as high as possible to get the best results. However, the strength of meteor

radars is that they are able to take measurements at all times during the day and in all weathers (Hibbins, 2015). This outperforms optical systems which requires daylight and a clear sky.

The SKiYMET meteor radar in Trondheim is a new-generation system, which was installed in the autumn of 2012. Instead of only one antenna it consists of eight antennas placed in a circle. The combined operating power of the antennas is 30 kW. The transmitted signal has a frequency of 34 MHz with a sampling frequency of 1 kHz. Further, the spacing between the antennas is 1.5λ. This is chosen so the transmitted signals will be phased to achieve constructive interference within the zenith angle of 15°-50°. Nodes of destructive interference is produced under 15° and above 50°. This specific angle range is selected due to the high amount of useful meteor detections (de Wit et al., 2014). Useful meteors are meteors whose position is determined unambiguously, and whose trails provide good enough measurements to be used in calculations.

The reflected beam is detected by five receiver antennas using interferometry. The receiver antennas are placed in an asymmetrical cross. The spacing between the middle antenna and the one at the north and the west is 2λ, while the spacing is 2.5λ between the middle and the other two (Hocking et al., 2001). This is done to obtain higher detection accuracy. For a given signal from a meteor detection, each pair of antennas will give an output. If the outputs agree well with each other the meteor observation is considered good enough to be used in calculations. If the detections from all the antenna pairs differ the meteor observation is dismissed. More details on the layout of components and how the SKiYMET meteor radar calculates the different parameters is described in (Hocking et al., 2001).

Back to the analysis, to decide the background wind speed at the location of a meteor, the radial velocity of the meteor trail was studied. Then two assumptions were made, one that the wind field was uniform and the other one that the vertical wind speed was much smaller than the horizontal wind speed. After filtering out all the unsatisfactory detections, a horizontal wind speed profile was calculated. Higher quality results were obtained by pre-defining a time and altitude range. Which was where the number of meteors was just enough to get sufficient data to work with, but not more. This was done to avoid including to many meteors which would bring noise into the data. Hence, a balance between the temporal and the spatial resolution was set. From the calculations a mean horizontal wind speed profile was worked out. The standard deviation from the mean for all meteors was also included. As for the wind profile below the meteor region, a reanalysis with data provided by the UK Met Office was done.

The high-frequency GW momentum flux was determined by looking at the deviations in the radial velocities from the mean radial velocity. This velocity perturbation was assumed to be a result from GWs. A full description on how to calculate the GW momentum flux from meteor radars can be found in (e.g. Hocking, 2005; de Wit et al., 2014). From the vertical divergence in the GW momentum flux, an estimate of the GWF could be produced. The magnitude of the GW momentum flux that was found in this paper agreed well with other similar studies.

To look into the GW momentum flux in more detail, a 10-day moving average was calculated in the zonal direction. This was done to take account for some of the noise in the data. The average showed again a vertical divergence which followed a seasonal cycle. In other words, the GWF followed a seasonal cycle with a westward direction in winter and an eastward direction in

summer. An eastward peak in early January was also observed, which was a result of the major SSW that year. The seasonal variability in the GWF was explained in terms of the stratospheric filter. As explained in section 2.3, the stratospheric winds work as a filter stopping some of the GWs from propagating up to the MLT. In winter GWs with a westward phase speed are not stopped by the eastward stratospheric wind profile, and can propagate up to the MLT and deposit their momentum. Hence, a westward forcing is observed. This reverses in summer, which was in full agreement with the results. The GWF ranged from -240 $\pm$ 70 ms^{-1} day^{-1} in winter, to +380 $\pm$ 70 ms^{-1} day^{-1} in summer. Figure 2.7 shows the GWF (blue line) and the net zonal wind speed (black line), the latter being a measure of the stratospheric filter.

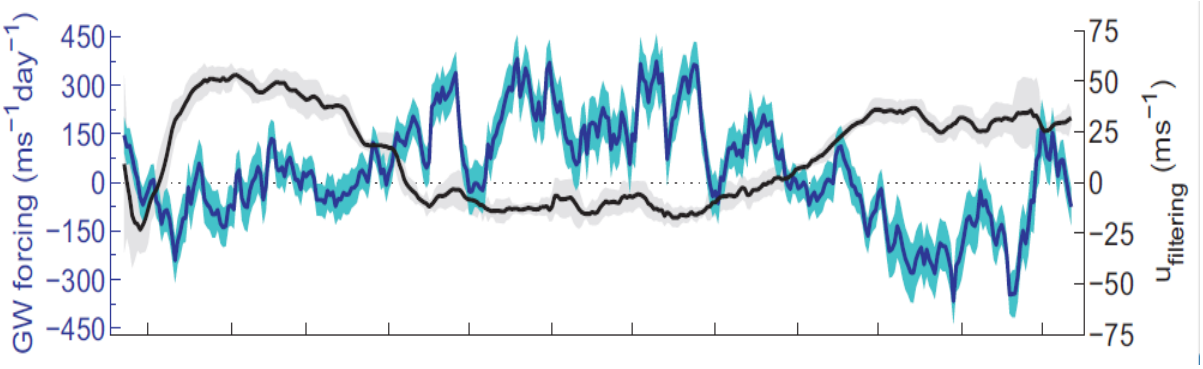

Figure 2.7: The 10-day moving averages of the GWF in the MLT (blue line), and the net zonal wind measured between the ground and 80.5 km (black line), with the uncertainties shaded (de Wit et al., 2014).

The net zonal wind speed is defined as the average between the most eastward and the most westward wind speed between the ground and 80.5 km. This number provided a measure of how eastward or westward the stratospheric filter was. It was found a negative correlation of -0.66 between the net zonal wind and the GWF, which was significantly correlated above the 99% confidence level. It was also found that the net zonal wind could be used to predict the GWF; an increase of 1 ms^{-1} in the net zonal wind led to a decrease of 4.6 $\pm$ 0.3 ms^{-1} day^{-1} in the GWF.

As shown in figure 2.7, the GWF followed a seasonal cycle but there was some high frequency variability present as well. This high frequency component was a result of something else than the seasonal stratospheric filter. This paper suggested that this could be caused by the influence of background winds in the mesopause, GW generation over the Scandinavian mountain range or in the stratosphere. Therefore, in this thesis, the high frequency variability will be studied in more detail, mainly by analysing the zonal and the vertical winds below the MLT on a daily basis.

Chapter 3

Data analysis

3.1 Pre-processing of the MERRA data

The computer program MATLAB R2014a version 8.3.0.532 was used to perform the analysis on Windows 7. The area of interest was set to Trondheim (63.4°N, 10.4°E) according to where the GWF was measured. Due to the grid structure in MERRA, the values used in this analysis were the average values calculated from the four nearest grid points surrounding Trondheim, see figure 3.1.

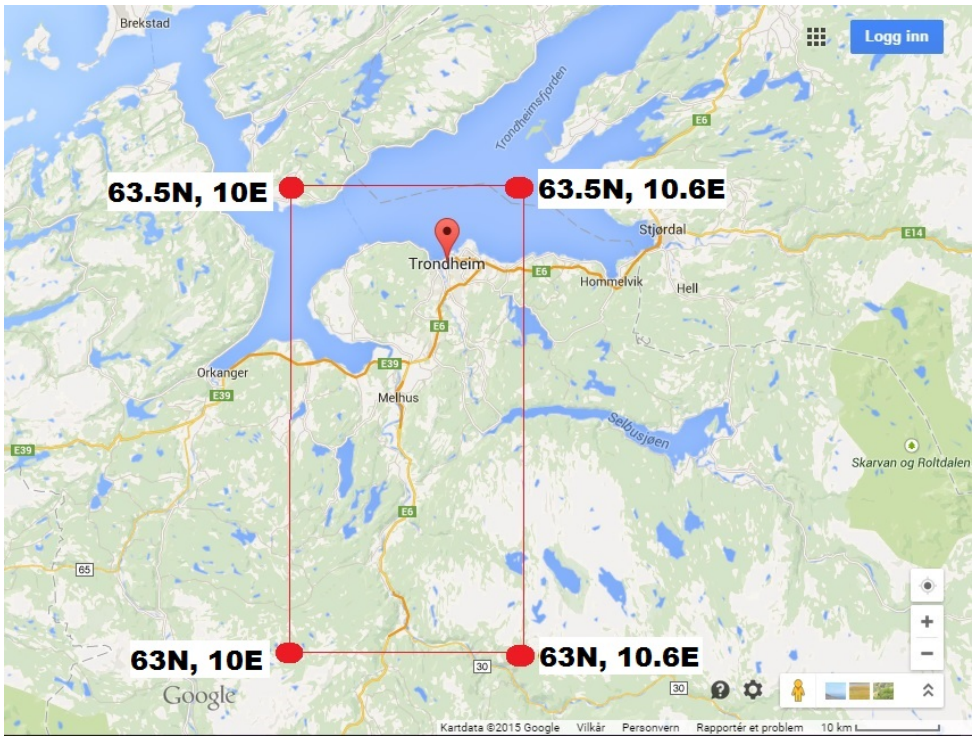

Figure 3.1: The four nearest points surrounding Trondheim, shown as red dots, in the MERRA grid structure (made from Google Maps, 2015).

Since MERRA uses both observational data and numerical models it was important to check if the output values were sensible. Typically in the boundary layers of a model i.e. at ground level/top level, the data can be set to unreasonable numbers so they will fit in the model. So

before starting the analysis a quality check was done to look for any extreme values, but none were found. As mentioned in section 2.6, the values were calculated on a six hour interval. So for each day four values were available. The average of these was then calculated to get one daily mean value. Finally, the analysis was divided into three parts:

1. Tropospheric wind variability
2. GW activity in the lower stratosphere
3. GW filtering

One thing to notice is that the start and end date for all of the data sets was January 6 2013 and December 26 2013, which gave 355 days in total. This was due to the 10-day moving average which the estimation of the GWF was based on (de Wit et al., 2014). The first five days and the last five days of the year were only used for calculations and did not get an averaged value of their own.

3.2 Tropospheric wind variability

In this part the region where GWs originate was studied in more detail. As mentioned in the background section, GWs are created in the troposphere and from there they propagate upwards. The aim was to find which altitude level in the troposphere that had the strongest connection with the GWF. By studying the variability in the tropospheric winds, a measure on the variability of the GW generation could be obtained. From the zonal and meridional wind speeds or u and v, the absolute wind speed w was calculated from equation 3.1.

$$w = \sqrt{u^2 + v^2} \tag{3.1}$$

This was then repeated for all the altitude levels between the ground and 200 hPa, covering the troposphere. The lower part of the stratosphere was not included to avoid that any seasonal trend here and in the MLT would contribute to a higher correlation. Then, the absolute wind speed at every altitude in this range was calculated. Finally, at each altitude, the 355 values for the absolute wind speed were compared with the GWF.

3.3 GW activity in the lower stratosphere

In this part the kinetic energy (KE) of the GWs was estimated by looking at how the wind speed varied as a function of altitude. The KE in the lower stratosphere will be a measure of the available KE of the GWs that had made it up through the troposphere. Hence, how much energy that could propagate higher up and influence the MLT. So the variability in this energy was therefore analysed to see if it could be related to the GWF.

Information about the wind speed between 0-30 km above Trondheim was taken from radiosonde data. As mentioned in section 2.5, radiosondes are launched twice a day at 00UTC and 12UTC (1 am/2 am and 1 pm/2 pm according to wintertime/summertime) from Ørlandet, about 50 km northwest of Trondheim. The lower altitude limit was set to 15 km to stay clear off the temperature minimum at the tropopause. The wind speeds tend to follow this rapid change

in temperature, and any sharp changes in the data could make the analysis more difficult to perform. So this region was therefore avoided. Further, the upper limit was set to 22 km according to the scientific paper by Moffat-Griffin et al. (2011), which completed a similar analysis in the Antarctic. This limit was chosen after they had studied the height where the balloons burst. This showed some seasonal trends, so a compromise between reducing these trends and have sufficient measurements, they only included balloons that reached at least 22 km. Also this range spanned more than a typical GW wavelength, thus, the entire wave could be studied and not just parts of it.

The total amount of missing launches or balloons bursting before reaching 22 km was 29% (206 of 710 possible). March and April had many unsuccessful launches, while July, August, September and October only had a few. December had the highest lack of measurements, with 80% missing. Figure 3.2 shows the amount of successful launches per month for the two launching times.

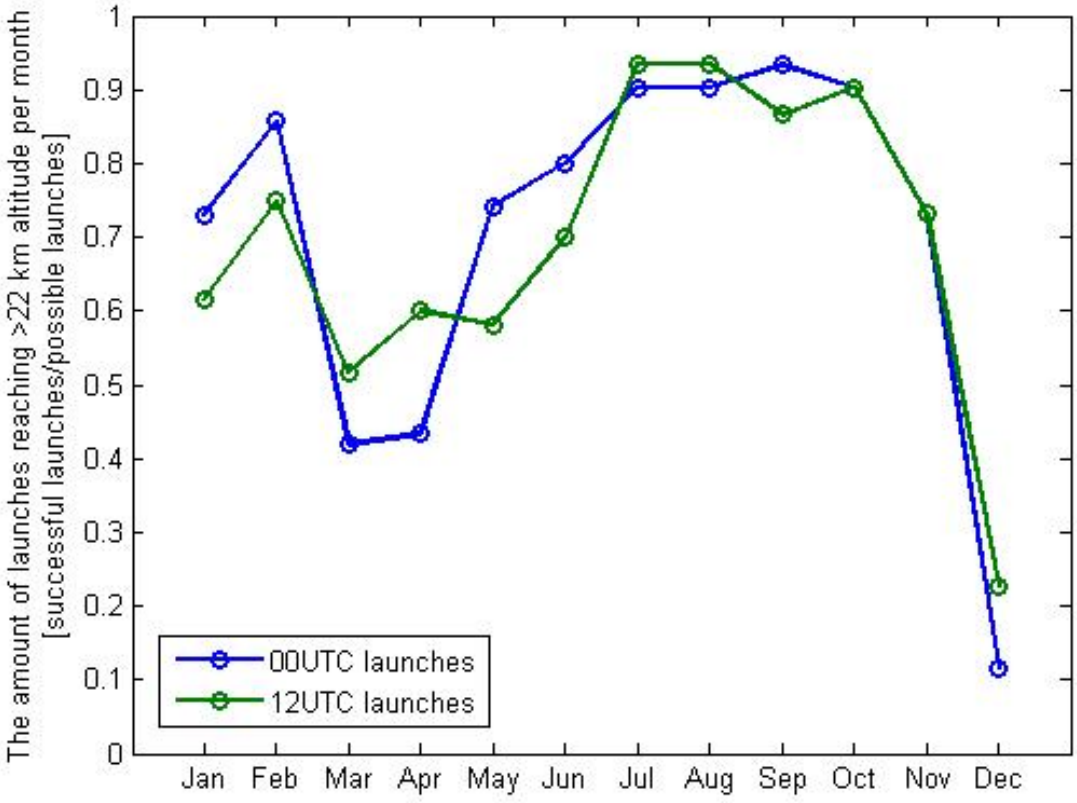

Figure 3.2: Of all the weather balloon launches from Ørlandet per month in 2013, the amount that made it above 22 km altitude, defined as successful launches, is indicated by the blue (00UTC) and the green (12UTC) lines.

For each successful launch the wind speeds within the set altitude range were taken out. To remove the background wind and only look at the high frequency variability, the steps in (Moffat-Griffin et al., 2011) were followed. By calculating a second order polynomial fit to the wind profile and subtracting this fit off, the high frequency variability was revealed (Vincent et

al., 2000). This was assumed to be a result from GW perturbation. Figure 3.3 shows an example of a wind speed profile and a wind perturbation profile, the latter called residual in the figure.

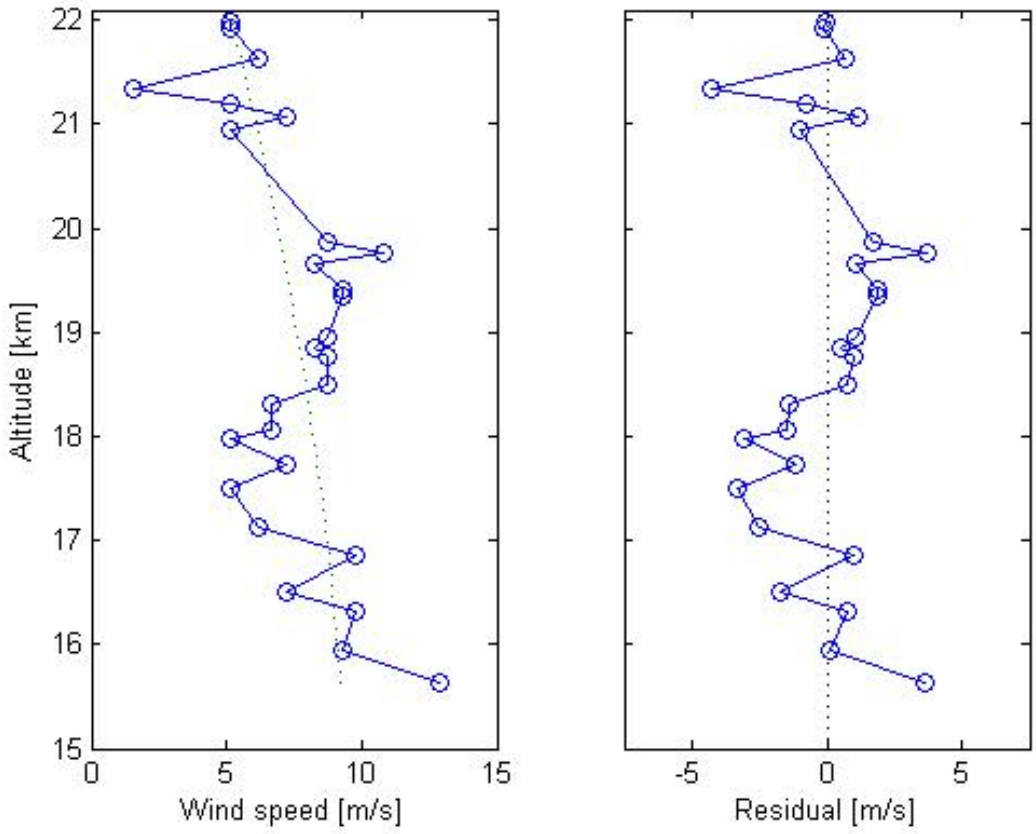

Figure 3.3: The plot on the left side shows the wind speed profile (blue line) with the polynomial fit (dotted line). The plot to the right shows the residuals (blue line) where the polynomial fit is removed. Based on radiosonde data from July 1 2013.

By studying how the wind perturbation profile varied, the GW activity could be estimated. This was done by taking the variance σ^2 of the wind perturbation profile. This would be equal to the perturbation w' in this range. Next, the kinetic energy (KE) could be calculated by equation 3.2 (Moffat-Griffin et al., 2011).

$$\frac{KE}{m} = \frac{\sigma^2}{2} = \frac{w'^2}{2} \tag{3.2}$$

The KE was divided by the mass m, as this unit was considered to be most convenient. Also, with this unit a measure of the GW mass was not needed. Then the KE/m was calculated for each day for the two launches. Finally, the analysis was completed by correlating the values of the KE/m at 00UTC, 12UTC and a mean between these, with the GWF. The mean was calculated by averaging the value of the KE/m if both the 00UTC and 12UTC launches were successful. If only one of them were successful the value from that one was used.

3.4 GW filtering

In this part the zonal (eastward or westward) wind speed in the middle atmosphere was looked into as a measure of the atmospheric transmission of GWs. The motivation was to investigate if the variability here could be related to the high frequency variability in the GWF. Also, by performing the analysis on a daily basis rather than with a 10-day moving average (as in de Wit et al. (2014)), the thought was see if the already known relationship with the GWF could be improved.

The zonal winds between 0-80 km above Trondheim were extracted from MERRA. Then three vectors were made which contained the value of the daily maximum, minimum and net zonal wind speed. The net zonal wind speed was defined as the average of the maximum and minimum wind speed on that day. This worked as a measure on the atmospheric state by providing a value of how much westward or eastward the wind was. A plot of the maximum, minimum and net zonal wind speed during 2013 can be seen in figure 3.4. It can also be mentioned that the net zonal wind changed in accordance to how the stratosphere changed throughout the year. With eastward (positive) winds in winter and westward (negative) winds in summer. The SSW that occurred in early January can easily be seen as a drop in the plot. Furthermore, the net zonal wind here compares well to the net zonal wind in (de Wit et al., 2014), see figure 2.7 in the background chapter. Thus, this figure can be used as an indication that the MERRA data is of quality and has been adequately implemented in the analysis.

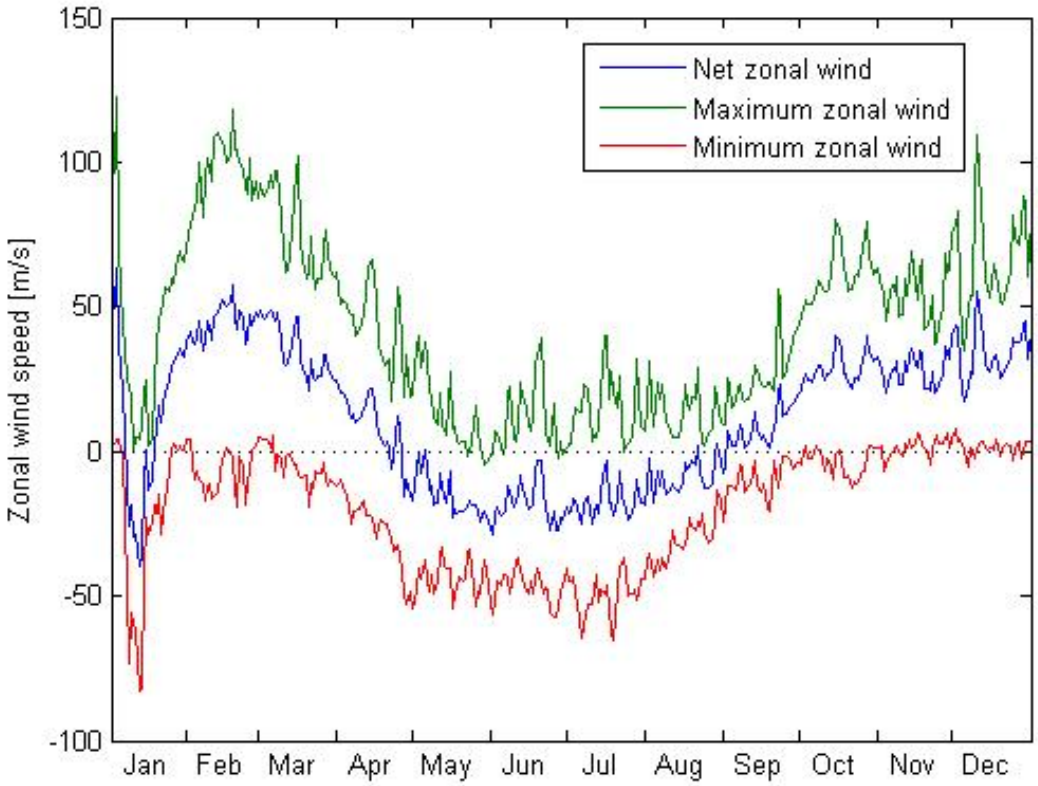

Figure 3.4: The maximum, minimum and average zonal wind speed, the latter defined as the net zonal wind. Based on MERRA data from Trondheim in 2013 between ground level and 80 km.

Moreover, the region between the maximum and minimum wind speed gave the blocking range. That was, GWs with phase speeds inside the blocking range would be stopped or absorbed by the background wind, while GWs with phase speeds outside the blocking range could propagate up to the MLT. Figure 3.5 shows a typical example of a winter stratosphere which is dominated by eastward (positive) winds. The vertical wind profile was taken from January 30.

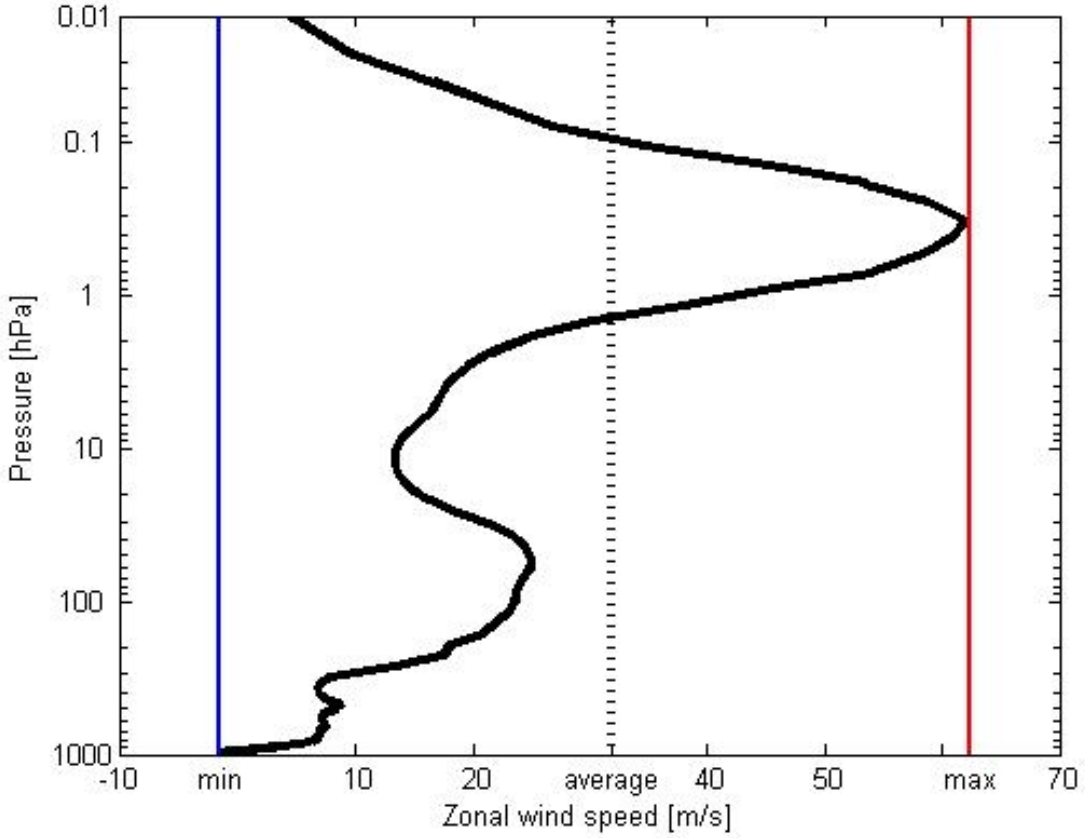

Figure 3.5: The minimum (blue line), maximum (red line) and their average, defined as the net zonal wind speed (black dotted line). The vertical profile between ground and 80 km of the zonal wind speed (black solid line) is based on MERRA data over Trondheim on January 30 2013.

To investigate more in detail what particular range of GW phase speeds that affected the MLT the most, an additional correlation study was done. The idea was to theoretically launch a uniform spectrum of GWs from the ground each day with speeds inside a specific range, say $\pm$ 20 m/s. And then use the MERRA data to find out how many of these waves that could theoretically propagate upwards without being stopped or absorbed by the background wind profile (i.e. the stratospheric filter) on that day. In other words, counting the GWs that was outside the blocking range. Each GW with positive (eastward) speed that made it all the way up was given a value of +1, and each GW with negative (westward) speed was given a value of -1. The sum of these two gave a number which was called the net GW number. This number was correlated with the GWF. Finally, the correlation was repeated for ranges going from $\pm$ 1 to $\pm$ 200 m/s.

Chapter 4

Results and discussion

4.1 Tropospheric wind variability

Figure 4.1 shows a plot of the absolute wind speed at different altitudes in the troposphere, which is ground level to about 15 km. The wind speed was sampled every third day from the MERRA data.

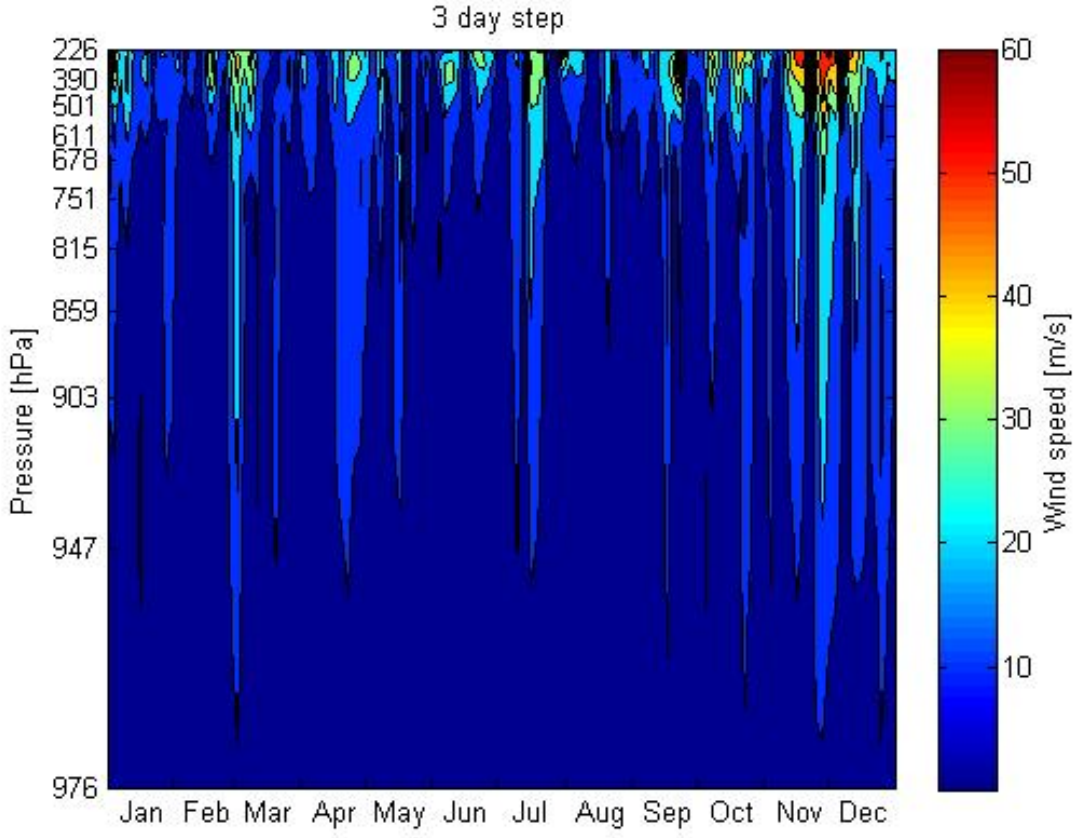

Figure 4.1: The absolute wind speed (in color) at different altitudes in the troposphere, sampled every third day in 2013.

This plot illustrates the large variability found in the tropospheric winds as they are influ-

enced by the highly variable weather. There were no particular trends that could be seen, except that the wind speed maximised in the top where the tropopause is. Here the wind speed reached as high as 60 m/s. At ground level the wind speed did not exceed $\sim$10 m/s.

The comparison of the absolute wind speed in the troposphere and the GWF throughout 2013, revealed small and negative correlation coefficients at each altitude level. The values went from -0.1300 to -0.2865, all significant above the 99% confidence level. The highest value of -0.2865 was found at the second lowest altitude level at 962 hPa. From this, 8.2% of the variance in the GWF could be related to the tropospheric wind variability.

Even though the correlation coefficients were all rather small, a study to investigate if seasonal trends had contributed to the correlation was performed. This was done by filtering the data. The filter used was a high pass Butterworth filter taken from the Matlab package; see the recipe in Appendix A. This filter was designed to pass any high frequency components with periods of less than 50 days, and stop frequencies with periods of more than 90 days. Hence, all the seasonal trends spanning more than three months were filtered out. The filter was applied to the GWF as well. Then the correlation procedure was run again. The results now showed very small correlation coefficients in the range from -0.06 to 0.03, with no significance above the 99% confidence level. Figure 4.2 shows a plot of the correlation coefficients without filter (blue line) and with filter (green line).

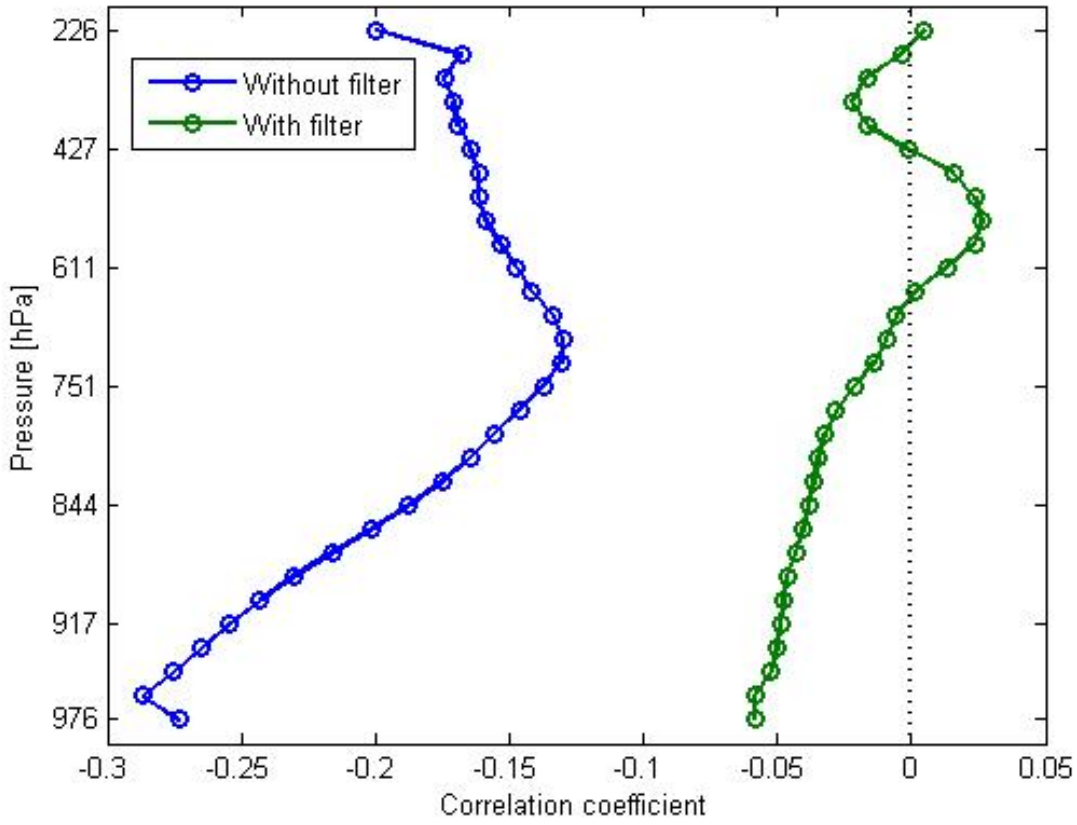

Figure 4.2: The unfiltered (in blue) and filtered (in green) correlation coefficients between the absolute wind speed at different altitudes in the troposphere and the GWF in the MLT in 2013.

From the figure it can be seen that the highest correlation coefficients were found at the lowest altitude levels, with and without the use of the filter. When going higher up, a decrease was seen which was followed by a small increase for both graphs. The filtered correlation coefficients seemed to have a wavelike structure towards the top of the figure. Because this was centred on the zero correlation line it was not given too much attention in the interpretation of the results. Also since the correlation coefficients decreased and became insignificant when filtered, it could be argued that the absolute wind speed in the troposphere had a low to no relation with the GWF. The small correlation that first was found was most likely a result from the seasonal variability in both the troposphere and in the MLT. Hence, the GW generation in the troposphere could not explain the high frequency variability observed in the GWF in the MLT.

4.2 GW activity in the lower stratosphere

4.2.1 Quality control of the radiosonde data

To begin with a few studies were done to look into the quality of the radiosonde data that was used in this part of the analysis. First, the monthly means of the KE/m (kinetic energy per unit mass) of the GWs was calculated from the radiosondes. This provided a measure on the GW activity in the lower stratosphere. Figure 4.3 shows the KE/m measured from the radiosondes that were launched at 00UTC and 12UTC from Ørlandet. The average between them was also calculated. They were all very similar, the only notable difference was found in December. This was most likely a consequence of the low number of successful launches or the poor temporal resolution that month as mentioned in section 3.3.

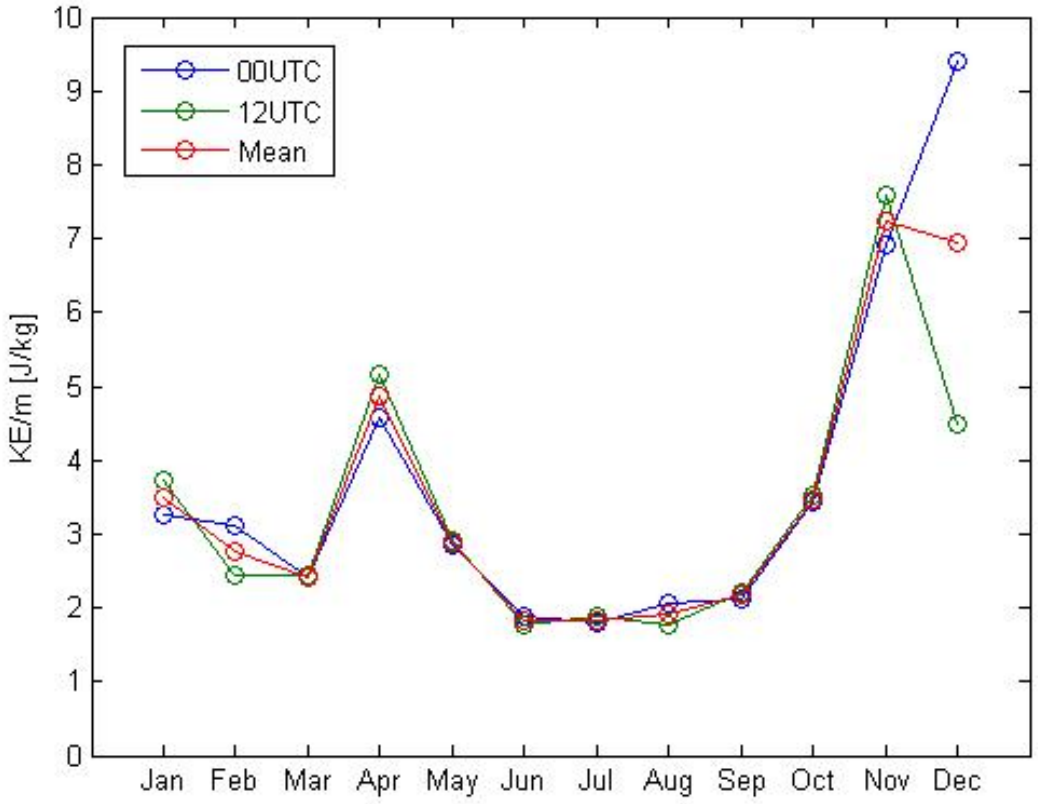

Figure 4.3: The monthly values of the KE/m (kinetic energy per unit mass) for the GWs, which is a measure of the GW activity in the lower stratosphere. Based on data from radiosondes that were launched at 00UTC (blue line) and 12UTC (green line) from Ørlandet in 2013. A daily mean value is also included (red line).

Apart from April, November and December where the KE/m peaked, it was rather stable with values between 2-4 J/kg. This is comparable to a study by Yoshiki et al. (2000). Radiosonde data from various launching sites around the world including Ørlandet, were analysed during a 10 year period. Their plot of the KE in the lower stratosphere was mostly flat from May to September. Then the KE increased to a maximum in January before it decreased until April/May. The flat period compares well with this analysis. On the contrary, the highest values found in November/December here, do not coincide with theirs found in January. Furthermore, the large peak in April that was found in this analysis does not appear in theirs. This was probably due to the temporal resolution in this data set was rather poor some months, while they have looked at the interannual variability with the average from 10 years of data.

Then the vertical resolution of the radiosonde data was examined. This was done to look for any seasonal trends that could possible interfere with the analysis. The vertical resolution was defined as the number of measurements taken by the radiosondes as they ascended, since the provided radiosonde data was not measured on a uniform vertical interval. In other words, the number of measurements taken by the radiosondes as they moved up through the atmosphere, varied. Figure 4.4 shows a plot of the vertical resolutions in monthly means at the 00UTC and 12UTC launches. The daily values can be found in Appendix B. The yearly mean was

20.2 and 20.6 measurements between 15 km - 22 km (i.e. 2.8 and 2.9 measurements per km) for the 00UTC and 12UTC launches respectively. Further, both graphs show that in April and December (also March for the 12UTC launches) that the number of measurements was at its lowest. So the poorest vertical resolution was found in these months.

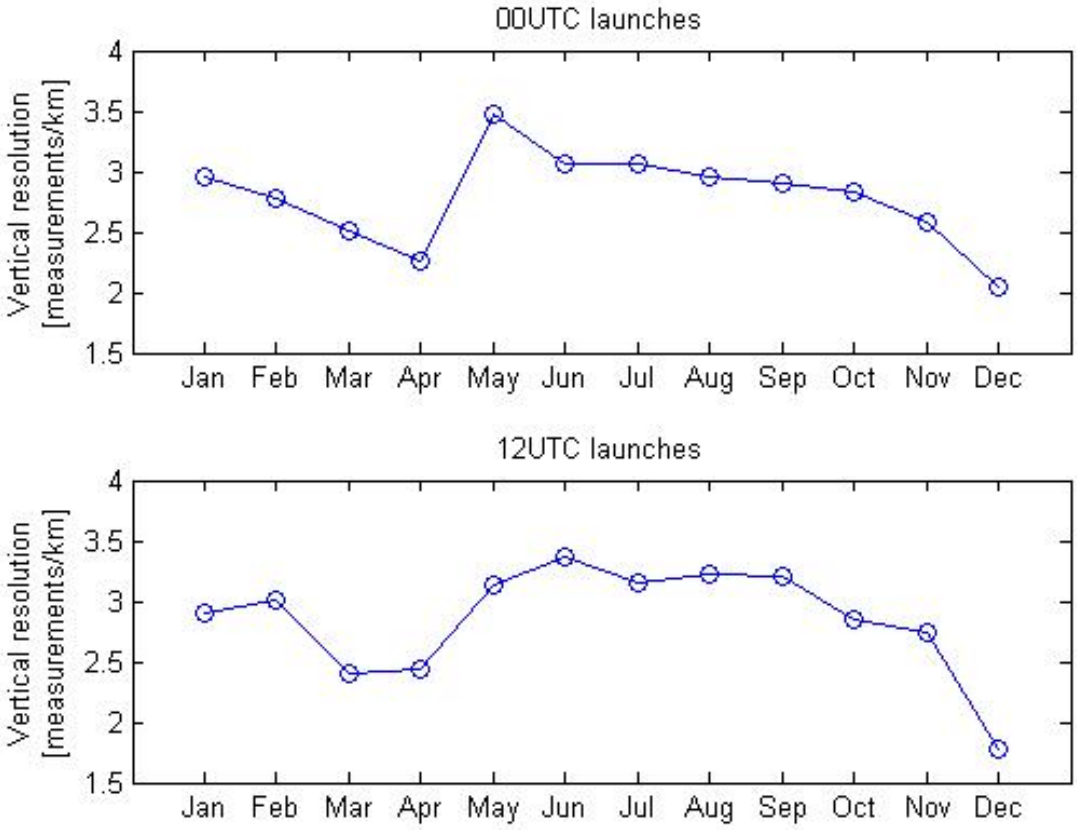

Figure 4.4: The vertical resolution, defined as the number of measurements per km taken by the ascending radiosondes, calculated on a monthly basis in 2013. The radiosondes were launched twice a day from Ørlandet at 00UTC (top) and 12UTC (bottom).

An interesting aspect was found when comparing these graphs with the graph showing the monthly mean values of the KE/m. For the 00UTC launches the KE/m peaked in April and in November/December. The same peaks could be seen for the 12UTC launches, except in December where the KE/m dropped. At first sight, there appeared to be a coupling between a low number of measurements and an increase in the KE/m. This was investigated further by looking at the correlation between the monthly mean KE/m and the vertical resolution. This showed a significant correlation above the 99% confidence level of -0.7286 and -0.5296, for the 00UTC and 12UTC launches respectively. However, when the same correlation performed once more on a daily basis, the results came out as small positive correlations, 0.0303 and 0.0418, that were not significant. The interpretation of this was that the connection between the vertical resolution and the KE/m was not significant, since the daily resolution revealed none. Even though a connection was found on a monthly basis this was most likely a result from random association.

4.2.2 Results from the correlation study

The main results from the correlation study with the KE/m (GW activity) in the lower stratosphere and the GWF, can be seen in table 4.1. The correlation coefficients did not vary much from each other and were all significant above the 99% confidence level. The highest correlation coefficient was with the daily mean with a value of -0.2958. In this case, 8.7% of the variance in the GWF could be explained by the variability in the KE/m.

	Correlation coefficient	p-value
00UTC	-0.2848	$4.1 \cdot 10^{-6}$
12UTC	-0.2857	$4.2 \cdot 10^{-6}$
Daily mean	-0.2958	$1.9 \cdot 10^{-7}$

Table 4.1: The correlation coefficients and their p-values between the GW activity in the lower stratosphere (KE/m) and the GWF in the MLT in 2013.

A plot of the GWF versus the daily mean KE/m can be viewed in figure 4.5. See Appendix B for the KE/m at the 00UTC and 12UTC launches.

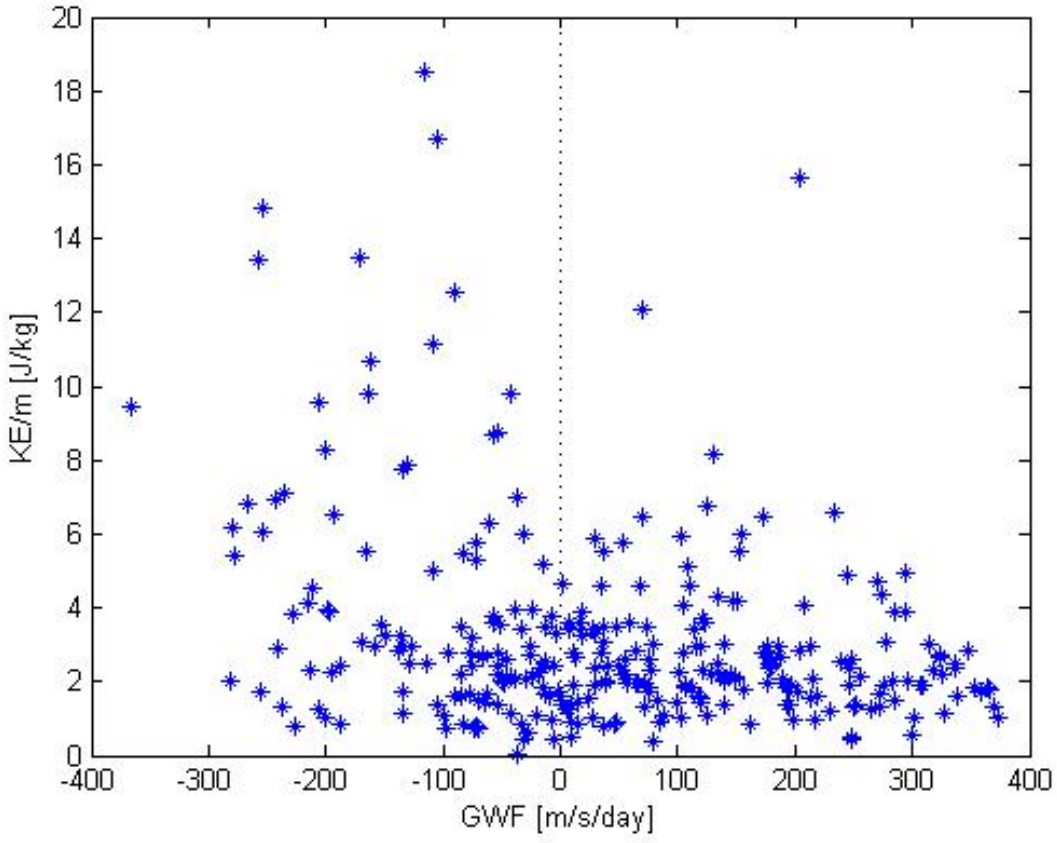

Figure 4.5: The GWF in the MLT versus the daily mean KE/m (GW activity) in the lower stratosphere in 2013.

At the bottom of the figure a cluster of points was found. The KE/m had values between 0 and 4 J/kg, and the GWF went from -300 to +400 m/s/day. Above this flat cluster on the

negative side of the GWF, the KE/m extended all the way to about 19 J/kg. Whereas on the positive side it only reached about 8 J/kg, except from two data points. The highest value for the GWF was found on the positive side, when the GWF was eastward (which it is in summer). In winter the GWF reached a maximum of -300 m/s/day except from one single data point.

All in all, this illustrated that there was a difference between the positive and negative side of the GWF. With the highest stratospheric GW activity measured when the GWF was negative or westward (which it is in winter). So it seemed to be a difference between summer and winter. This apparent seasonal difference was then investigated. Due to the non-continuous temporal resolution (many days of missing launches), the high pass filter used in the previous section to remove seasonal trends, could not be applied here. In fact, it was rather hard to filter the data when many data points were missing. One way to do this was to interpolate between data points, but because many were missing in a row, interpolation was believed to provide unsatisfactory results. Another method was therefore needed to take account for these trends. This was solved by just looking at the summer months' worth of data for both the radiosondes and the GWF. Hence, only including one season in the analysis.

The summer stratosphere is characterised by westward winds, hence the GWF is mostly eastwards as described in section 2.3. From figure 4.6 the GWF was mostly eastward (positive) from April to August. For the radiosonde data, both the temporal resolution (successful launches) shown in figure 3.2, and the vertical resolution shown in figure 4.4, were at their best in May/June to October. Also the values of the KE/m was rather flat without any trend or low frequency variability in this period, see figure 4.6. With this in mind, the summer season was chosen to go from May to August, shown by the black vertical lines in figure 4.6. The temporal range was further extended to include August and September as well, as these were considered to be months with summer season trends present. This is shown by red dotted lines and with a red solid line marking the end date at October 1.

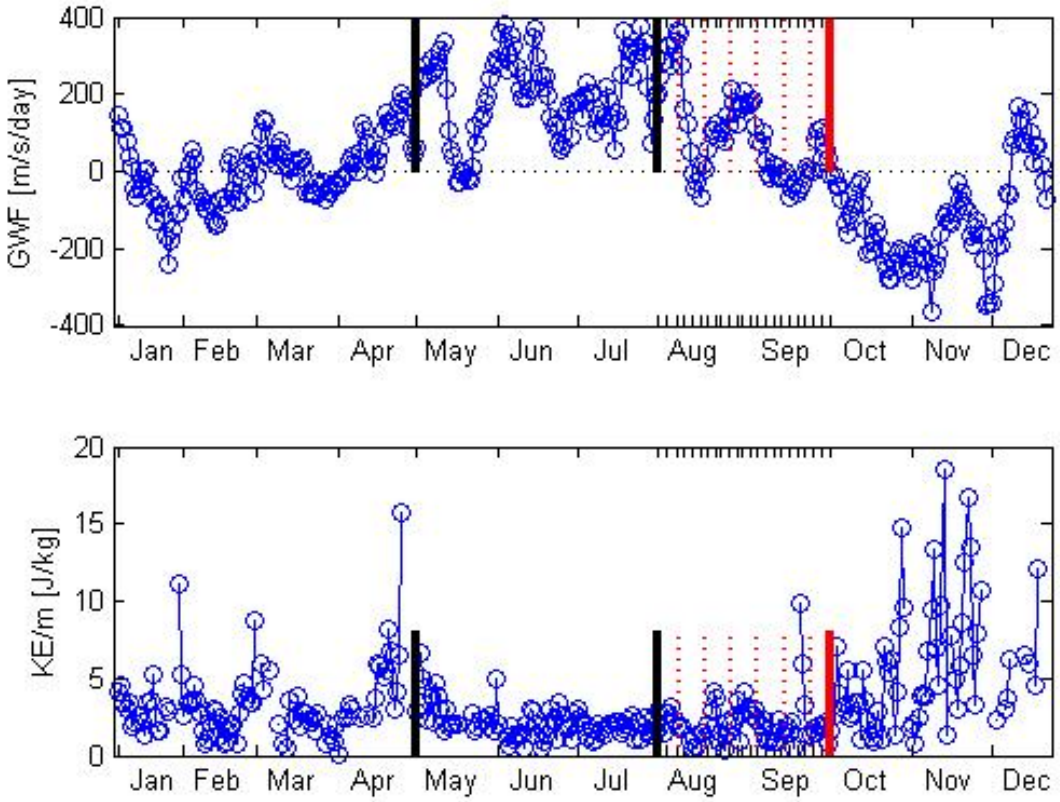

Figure 4.6: The temporal range used when comparing the GWF in the MLT (top), and the daily mean KE/m (GW activity) in the lower stratosphere (bottom), during the summer season. The summer season was chosen to be May 1 to July 31, indicated by the black solid lines. Then the range was extended in 1 day steps to include August and September as well. The red line illustrates the end point at October 1.

To see how the correlation changed for different temporal ranges the following procedure was followed. First, the correlation between the daily KE/m and the GWF in May, June and July was calculated. Next, the temporal range was extended in 1 day steps to include August and finally September. The correlation was calculated for each new included day, in total of 61 individual correlations. The result can be seen in figure 4.7.

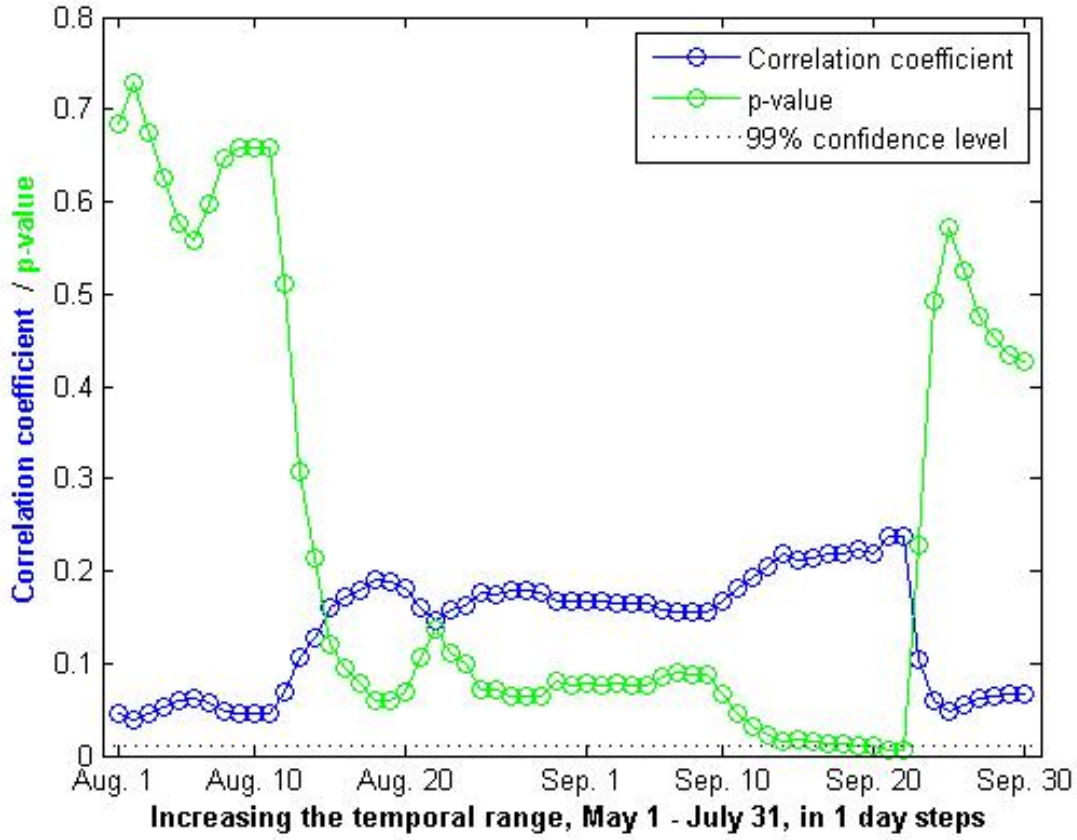

Figure 4.7: The correlation coefficients and their p-values between the GWF in the MLT and the GW activity (KE/m) in the lower stratosphere, when the temporal range, which started at May 1 and ended July 31, was extended in 1 day steps to include August and finally September. Going from the left to the right, each correlation coefficient and p-value correspond to a temporal range that was 1 day longer than the previous one.

From the above figure it can be seen that the correlations were rather small and mostly insignificant. The highest correlation of 0.2363 and significant at the 99% confidence level, was found with the temporal range going from May 1 to September 21 and 22. Compared to the first result the correlation coefficient went from -0.2958 to 0.2363. This can be understood in terms of seasonal variability. When considering the entire year of the KE/m values, it can be seen from figure 4.6 that the highest values were found in the winter months, especially in November and December. The lowest values were found in the summer months, May through September. This was the opposite when compared to the GWF. The GWF had its lowest values in winter and highest values in summer. Hence, a small negative correlation between the seasonality in the two graphs was seen. When only looking at the summer months, the high frequency variability for both graphs only marginally approached a significant correlation, as seen in figure 4.7. A high correlation between these two would indicate that they were related in small temporal scales, and not just on a seasonal basis. Since the correlations were small it was therefore reasonable to state that the variability in the GW activity could not explain the high frequency variability in the GWF. The relationship between them was strongly based on the seasonal cycle.

Having considered the individual correlation between part 1 and part 2 with the GWF, it could be interesting to look at the correlation between these two. A relation would be reasonable since the GWs that are generated in the troposphere, need to propagate through the lower stratosphere to get to the MLT. Therefore an extra correlation study was done. The aim was to see if any of the altitude levels in the troposphere were connected to the GW activity in the stratosphere. The result revealed correlation coefficients ranging from 0.3184 to 0.5008, significant above the 99% confidence level. With the highest value found at altitude level 8 and 9 from ground, or 874 hPa and 859 hPa. In this case, the tropospheric wind variability could explain 25% of the variability of the GW activity in the lower stratosphere. Figure 4.8 shows the correlation coefficients.

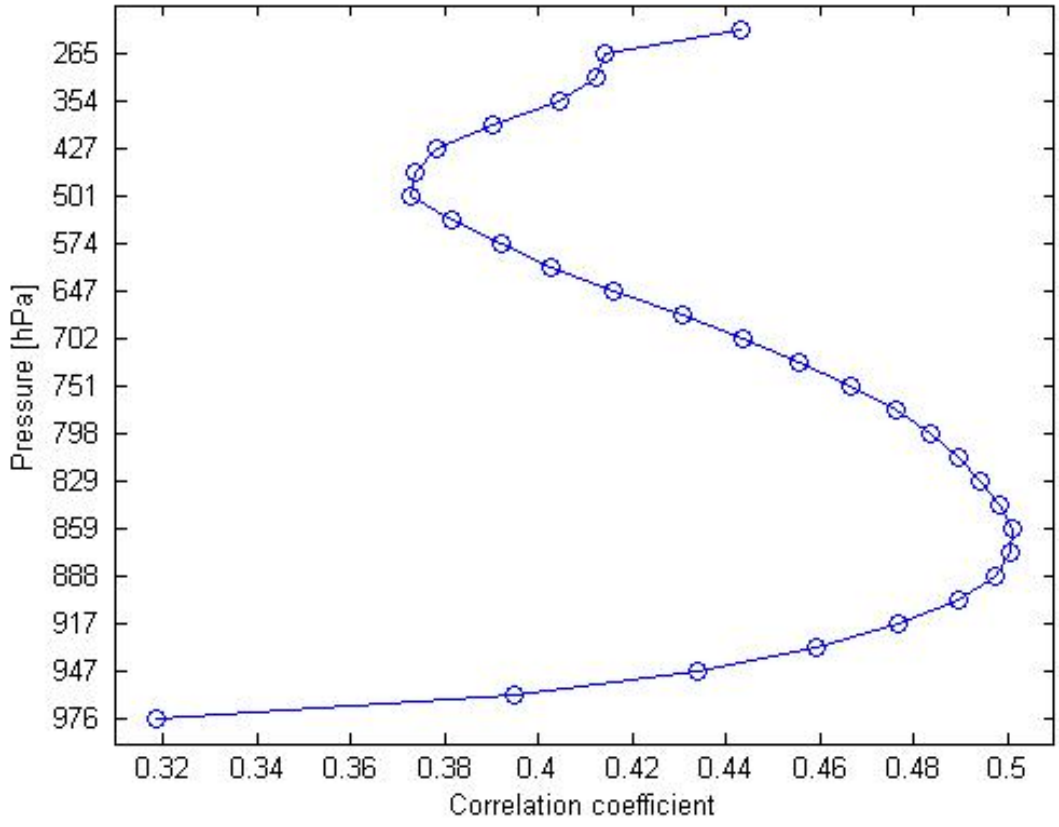

Figure 4.8: The correlation coefficients between the absolute wind speed in the troposphere and the GW activity (KE/m) in the lower stratosphere at various altitudes in 2013.

The lowest correlation coefficient was found at the ground. From there it increased to a maximum of 0.50 at 859 hPa, and then it decreased to a second minimum of about 0.37 at 501 hPa. From there and to the top of the troposphere at 265 hPa, a small increase was seen. Compared to the study by Yoshiki et al. (2000), which analysed radiosonde data over a 10 year period, this result was weaker. They namely found a strong correlation between the surface wind and the GW activity in the lower stratosphere. This is probably because they looked at 10 years of data, while this analysis only studied one year. As a final consideration, the same filtering method as explained above was applied to this part. The result when only looking at the summer months was that the correlation coefficients dropped and became insignificant. This was the case for all of the altitude levels, and at all temporal ranges. A contour plot of the

correlation coefficients can be seen in figure 4.9. The values ranged from -0.1 to 0.15 as shown by the colorbar.

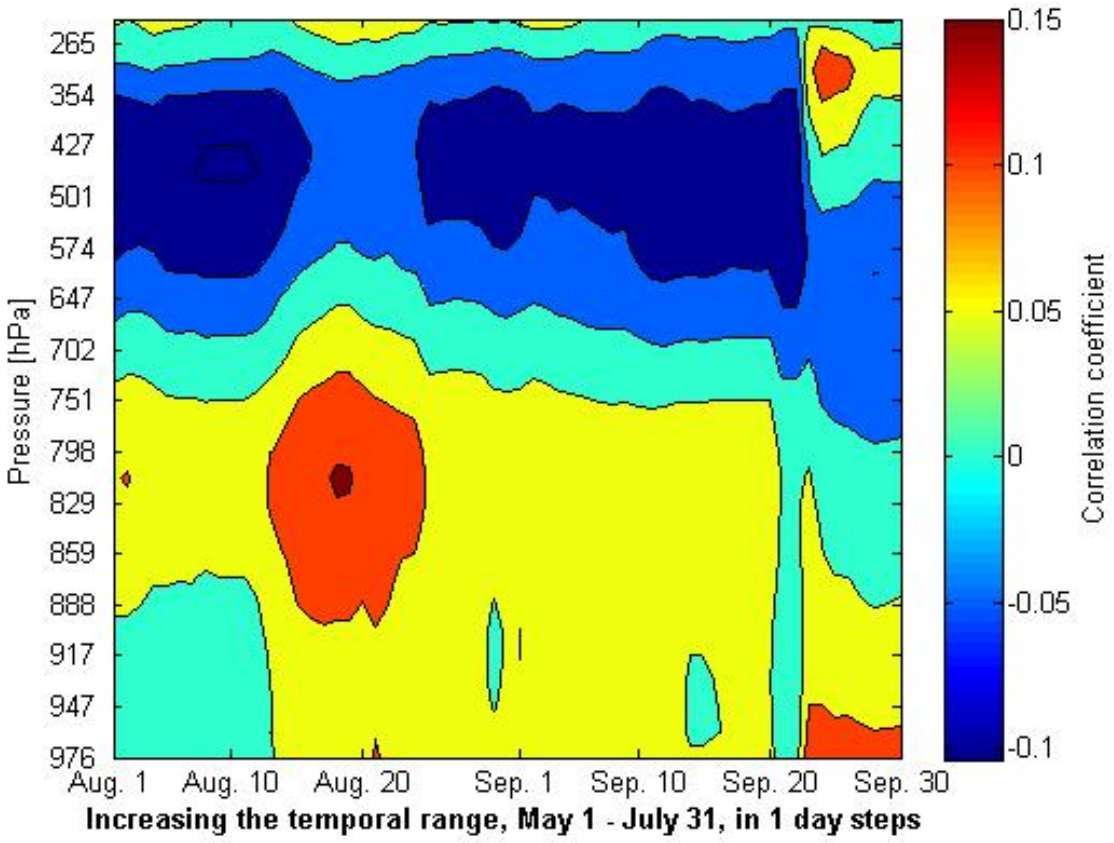

Figure 4.9: The correlation coefficients (in color) between the absolute wind speed in the troposphere and the GW activity (KE/m) in the lower stratosphere at various altitudes. The temporal range that started May 1 and ended July 31, was extended in 1 day steps to include August and September, to only consider the summer season.

The correlation coefficients changed from slightly positive to slightly negative at about 702 hPa. Some variability both in the vertical and the horizontal direction can also be seen. Because of the small and insignificant correlation coefficients no further analysis of this plot was done. To sum up, from the above figures it was reasonable to say that the relationship between the tropospheric wind variability and the GW activity in the lower stratosphere, came from seasonal variability. And even with the seasonality included, the maximum correlation coefficient did not exceed 0.5008.

4.3 GW filtering

The GWs generated in troposphere can be stopped (absorbed) from propagating higher up by the atmospheric conditions in the stratosphere (Fritts and Alexander, 2003), known as GW filtering. A measure of the stratospheric filter can be obtained by studying the wind speed direction. In brief, if the stratosphere has eastward winds, GWs with an eastward phase speed reaching this area will be absorbed. While GWs with a westward phase speed can propagate through and

reach the MLT. The net zonal wind, which is defined as the average between the most eastward and most westward wind between the ground and 80 km, will provide a value of how eastward or westward the atmosphere is, hence a measure of the stratospheric filter. When the daily net zonal wind throughout 2013 was compared to the GWF a correlation coefficient of -0.6472 was found, significant at the 99% confidence level. As a result, 42% of the variance in the GWF could be related to the variability in the net zonal wind. Compared to the results from de Wit et al. (2014) that used a 10-day moving average, the net zonal wind on a daily basis did not improve the correlation with the GWF, it was actually a bit smaller. Since it was the atmospheric state that filtered the GWs, and therefore decided which GWs that were allowed to propagate upwards and influence the GWF (e.g. Fritts and Alexander, 2003; de Wit et al., 2014), it could be expected that the correlation would be even higher. With that said, it could be stated that there was a connection between the opacity of the atmosphere below the MLT, and the GWF in the MLT. So the net zonal wind could account for some of the high frequency variability in the GWF, but not all. Figure 4.10 shows a plot of the GWF as a function of the net zonal wind.

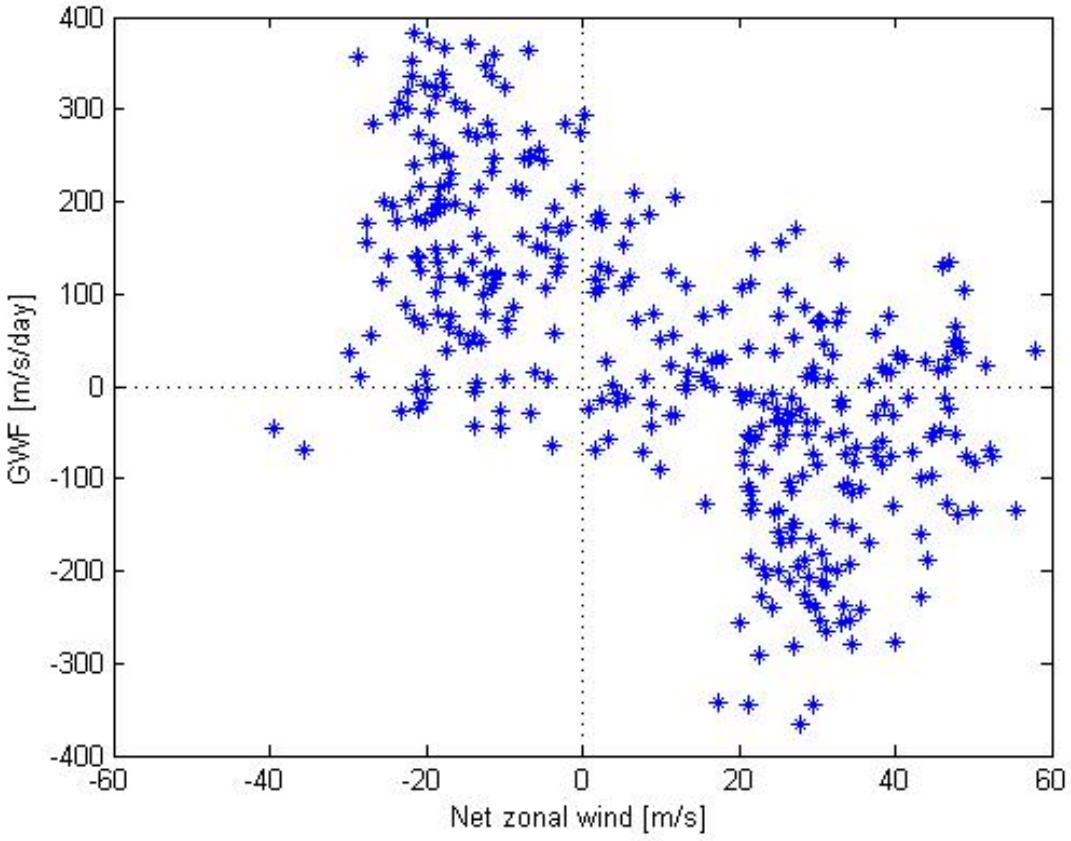

Figure 4.10: The GWF in the MLT as a function of the daily net zonal wind in 2013. The net zonal wind indicates how westward or eastward the stratospheric winds are, hence, it provides a measure of the GW filtering.

From the above figure it can be seen that the data points were not uniformly distributed but rather gathered in two clusters. One in the top left square and one in the bottom right square. Some outliers were seen in the top right level as well. Further, this figure indicates that the GWF experienced a positive or eastward forcing when the net zonal wind was negative or westward. The same can be said for the lowest right corner, with a positive or eastward net zonal wind and

a negative or westward GWF. This was in accordance with the knowledge about an eastward (westward) atmospheric state only passes westward (eastward) GWs to propagate to the MLT.

Then the same high pass filter from part 1 was applied to the net zonal wind and the GWF. The correlation dropped to 0.0462 and was no longer significant at the 99% confidence level. Which can be used as an indication that the relationship between the atmosphere below and in the MLT was most likely governed by the seasonal variability. A plot of the GWF as a function of the net zonal wind after the seasonal trends were removed can be seen in figure 4.11.

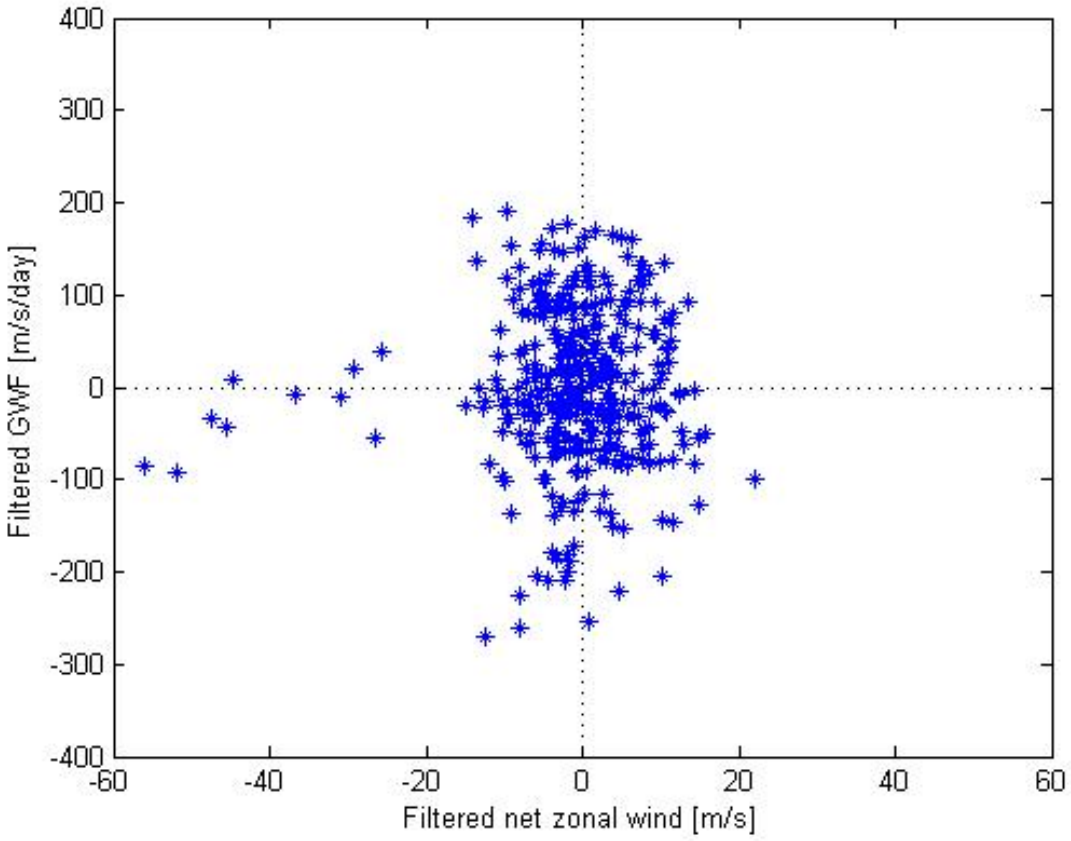

Figure 4.11: The GWF in the MLT as a function of the daily net zonal wind in 2013, after the seasonal variability was removed through filtering.

The data points were now more or less centred on the origin. This illustrated that without the seasonal component, the net zonal wind and the GWF had a low to no connection with each other. And could therefore not explain the high frequency variability in the GWF. In figure 4.12 a plot of the net zonal wind and the GWF as a function of time is shown. The upper graph was before the filter was applied, and the lower graph was after.

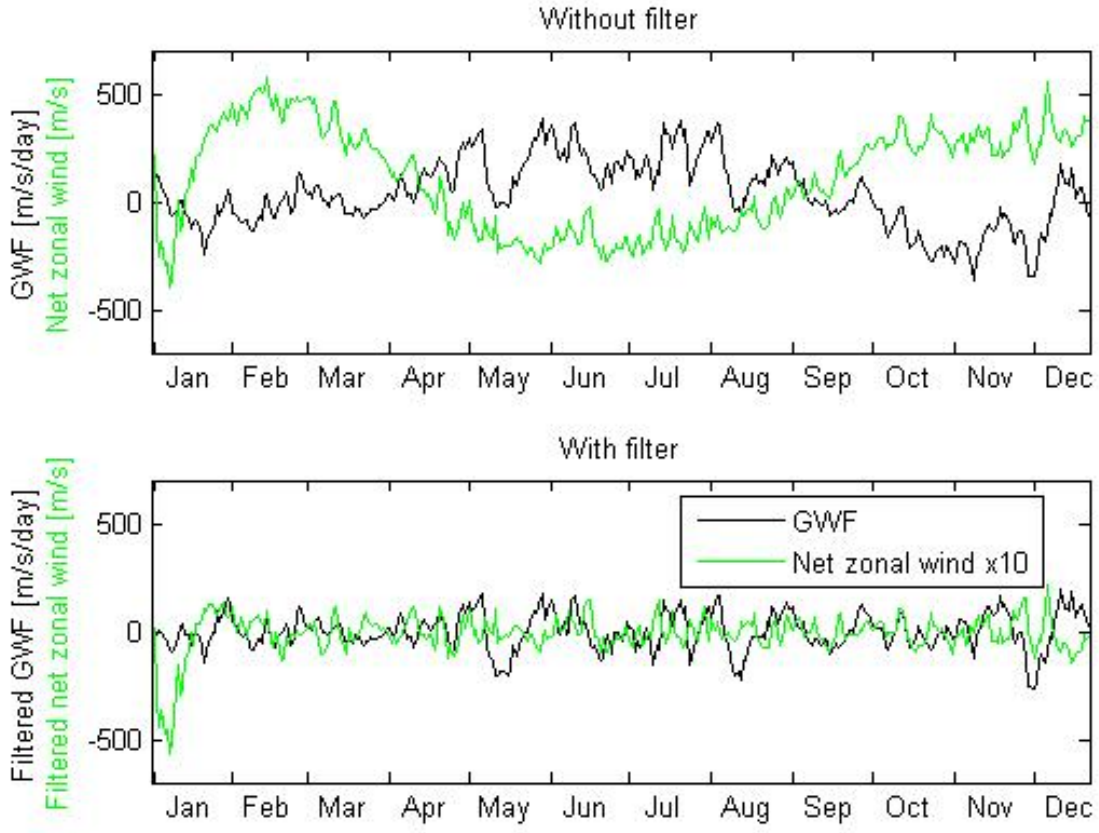

Figure 4.12: The GWF in the MLT (black) and the net zonal wind in the stratosphere (green), which is multiplied with 10 due to scaling, in 2013. With and without the seasonal filter applied.

The final correlation study looked into how the phase speed spectrum of GWs affected the GWF. GWs with phase speeds inside a set range, uniformly distributed around 0, were theoretically launched from the ground. And by using information about the GW filtering in the stratosphere, it was possible to find out how many of the GWs in the set range that could reach the MLT without being stopped by the stratospheric filter. Further, the range was changed to see if it made any difference on the impact felt in the MLT. The results showed that GWs with phase speeds within the range of $\pm$ 46 m/s obtained the highest correlation with the GWF. It was 0.6932 and significant at the 99% confidence level. In other words, the GW phase speed range that had the greatest effect in the MLT was found. In this case, 48% of the variance in the GWF could be explained by the variability of these GWs. Another thing to point out is that the result showed that by applying a restriction to the GWs, the correlation between the GWs and the GWF improved a little. It went from -0.6472 when only the stratospheric filter (net zonal wind) was considered, to 0.6932 when the stratospheric filter was combined with the GW phase speed range. To put it differently, it went from explaining 42% to 48% of the unfiltered variability in the GWF. Below, a plot of the correlation coefficients at the different phase speed ranges can be seen in figure 4.13.

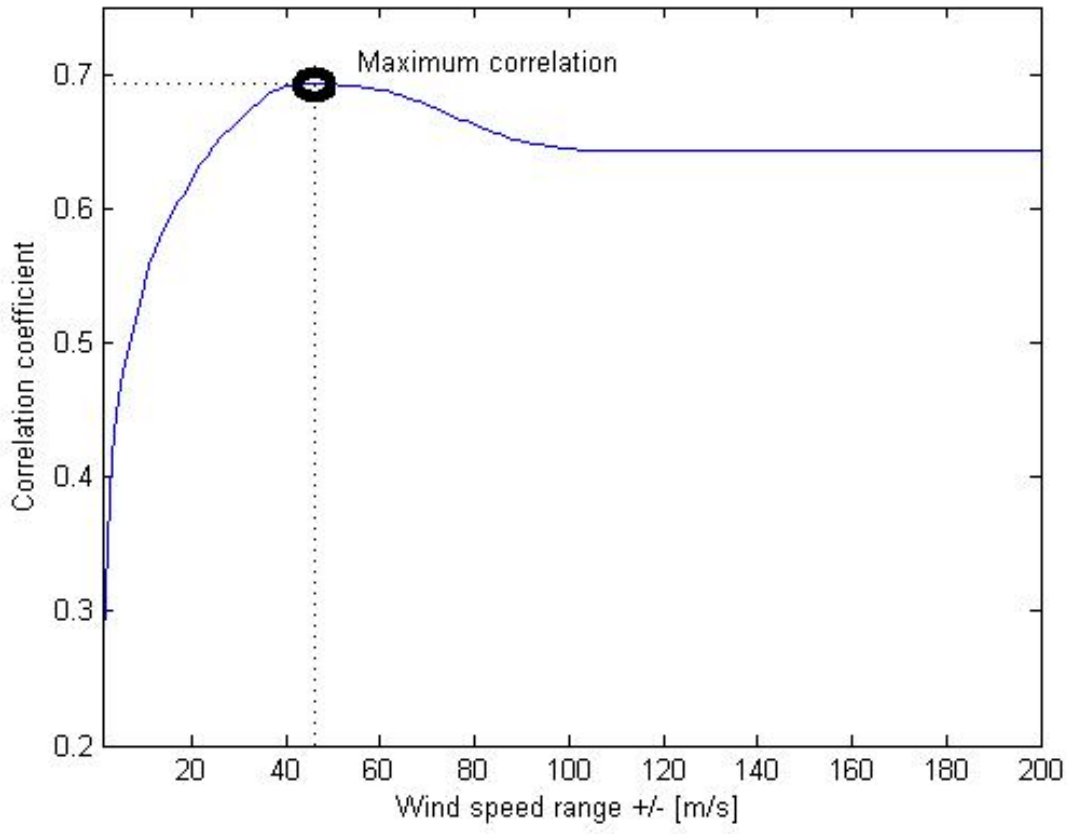

Figure 4.13: The correlation coefficient between the net GW number (defined as the amount of GWs that theoretically made it up to the MLT) for different phase speed ranges, and the GWF in the MLT in 2013. The best correlation was 0.6932 for GWs with phase speeds within the $\pm$ 46 m/s range.

The correlation coefficient increased up to $\pm$ 46 m/s and then it decreased just a little bit. After $\pm$ 100 m/s it was constant. To explain why the correlation coefficient behaved like this figure 4.14 can be helpful.

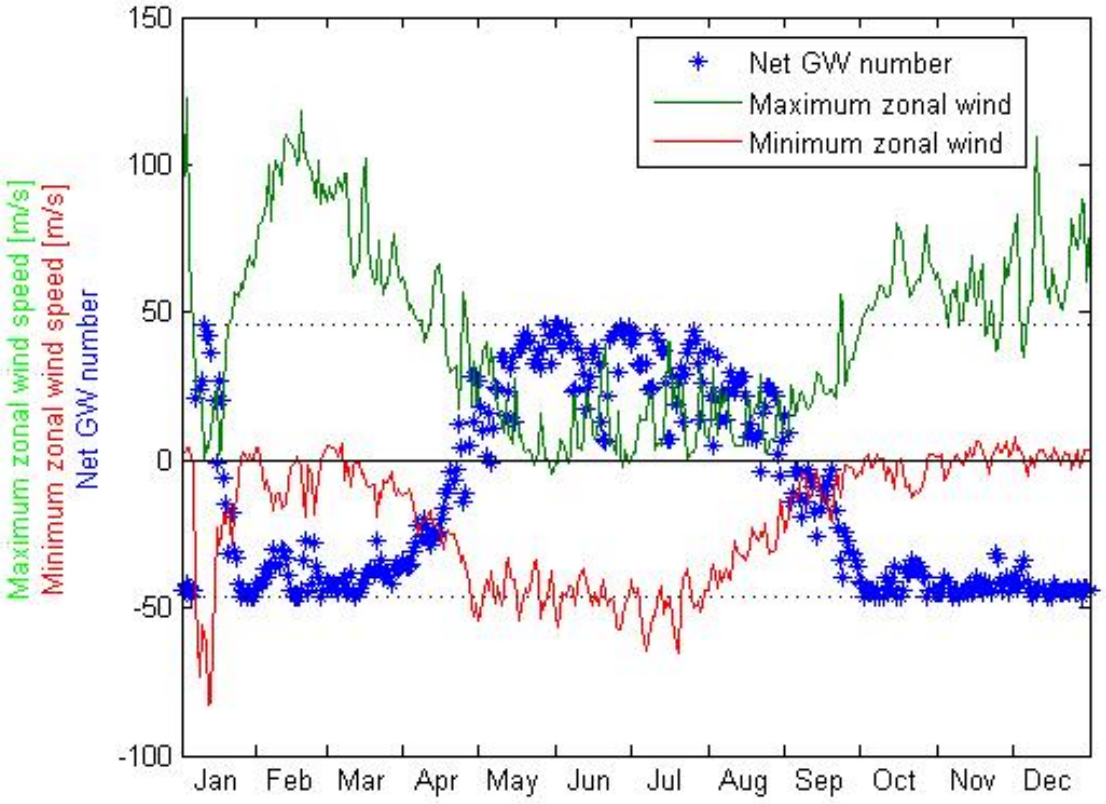

Figure 4.14: The net GW number (blue), which indicates the amount of eastward or westward GWs that made it up to the MLT, within the $\pm$ 46 m/s phase speed range (black dotted lines). The maximum and minimum zonal wind speeds in 2013 are illustrated by green and red lines.

For clarification the area between the green and red line illustrates the blocking area. This was where GWs with matching phase speed were absorbed. GWs with phase speed outside this range could propagate through, and would contribute to the net GW number. If the range, illustrated as black dotted lines in the figure, were too close to each other the number of launched GWs was low, and many would be stopped by the blocking range. When the range was extended, more GWs would be launched, and more would make it up and deposit their momentum in the MLT. So the correlation coefficient was seen to increase. After $\pm$ 46 m/s a small decrease was observed. This was because no new information about how the blocking range behaved was achieved. Look at February for example, if the range was extended to $\pm$ 60 m/s no additional positive GWs were allowed to pass since the positive blocking range went to about +100 m/s. On the contrary, more negative GWs were allowed to pass. The final result was just a more negative net GW number. The same applies for October to December. The opposite was seen in May to August. When the range was extended here, the net GW number became more positive. So to sum up, the shape of the blue dotted line would be more or less the same, but a bit stretched in the vertical direction when the range increased. Therefore, the tiny decrease seen in the correlation coefficient was probably caused by small changes when the shape of the net GW number was stretched.

Lastly when extending the range after $\pm$ 100 m/s the correlation coefficient became constant. This was due to the phase speed range now covered the entire blocking range on both sides. So all the eastward GWs would cancel out all the westward ones.

A scatter plot of the net GW numbers at the highest correlation range in 2013, and the GWF can be seen in figure 4.15. The first was multiplied with 10 to get them on the same scale.

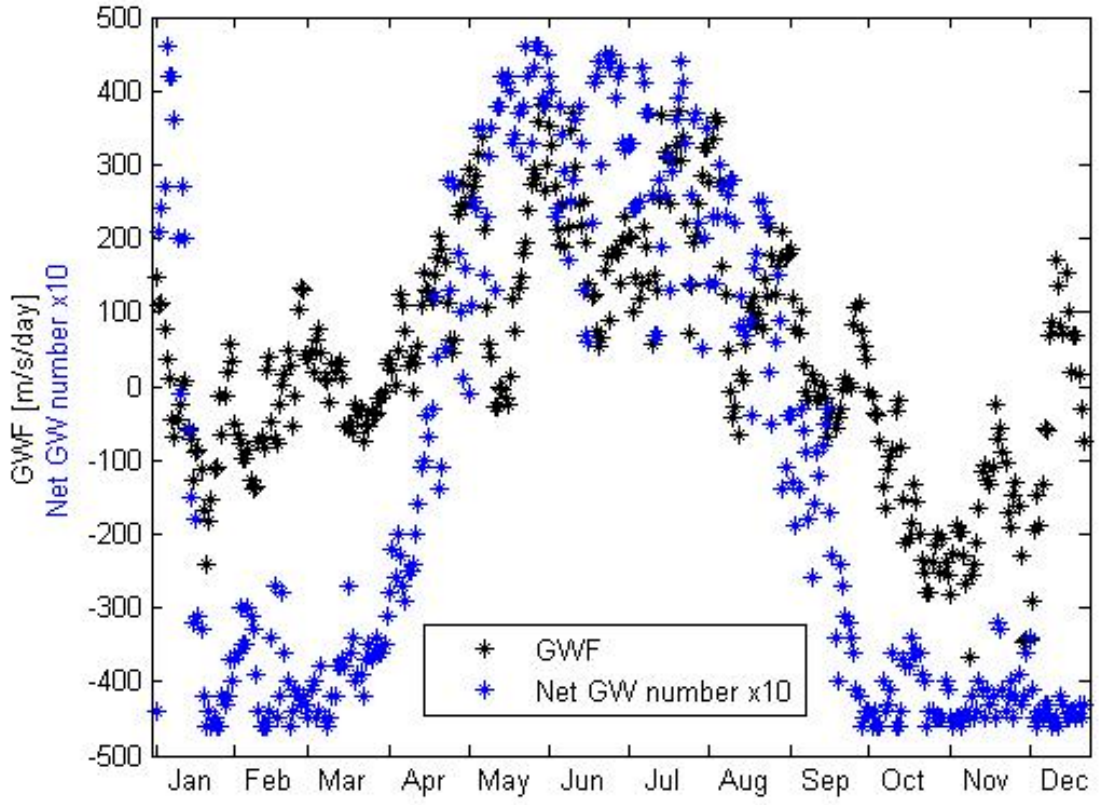

Figure 4.15: The GWF in the MLT (black), and the net GW number (blue) in 2013. The latter is multiplied with 10 for scaling reasons.

From this figure a seasonal trend can be seen for the net GW number, as would be expected knowing how the atmosphere behaves during the course of a year. In winter from October through March the net GW number was negative or westward. A positive peak in early January illustrated the large SSW that was mentioned in section 2.4. In summer from April through August, the net GW number was positive or eastward. As a final correlation study, the net GW numbers were filtered using the same high pass filter as in part 1. The result showed like before, that the correlation dropped and became insignificant when filtered, with a value of -0.0944. This indicated again that the apparent relationship was a result from seasonal variability. Figure 4.16 shows the net GW number and the GWF as a function of time before and after the filter was applied.

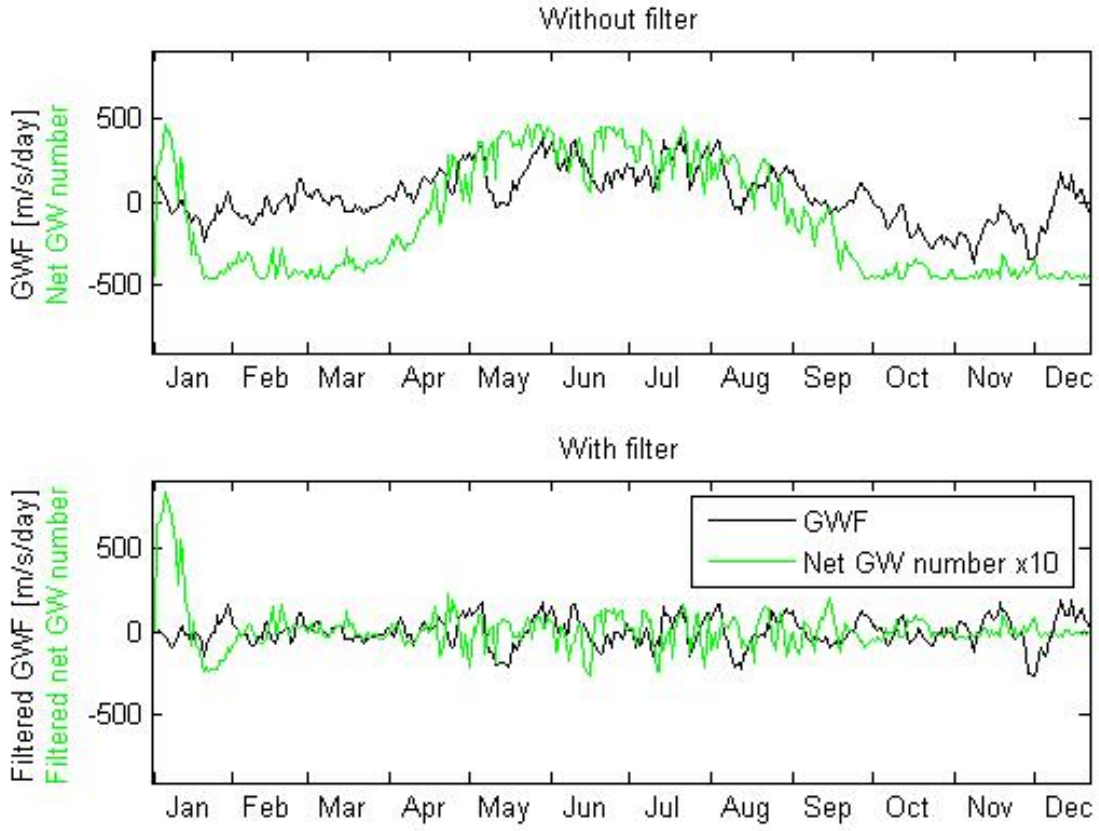

Figure 4.16: The GWF in the MLT (black) and the net GW number (green), which is multiplied with 10 due to scaling, in 2013. With and without the seasonal filter applied.

Although the analysis revealed small and insignificant correlation coefficients when filtered, the knowledge about what phase speed range that influenced the MLT the most, was interesting. As seen from the above results, the correlation increased a bit when combining the GW phase speed range with the stratospheric filter. In other words, this combination was able to explain more of the seasonal variability in the GWF before the filter was applied. This restriction on the GWs should be researched further to see if it could be used in weather and climate models to take account for the effects of GWs more accurately. Thus, improve the output from these models and in that way, make the models better. With that said the results from this analysis are indeed interesting. However, the main conclusion would be that the net zonal wind and the net GW number were related to the GWF on a seasonal basis. Hence, the high frequency variability in the GWF could not be explained in more detail by any of these.

Chapter 5

Conclusion and outlooks

In this thesis the high frequency variability measured in the GWF in the MLT was studied. With spatial and temporal limits confined to Trondheim (63.4°N, 10.4°E) in 2013. To explain the high frequency variability, three elements related to the GWs in the atmosphere below the MLT were considered on a daily basis. That was, the tropospheric wind variability which acted as a measure of GW source variability, the GW activity in the lower stratosphere which was measured by the kinetic energy per unit mass, and lastly the GW filtering which restricted the amount of GWs reaching the MLT. Information about the wind speed, which described the GWs, was taken from a climate model (MERRA) and from radiosondes. Then the correlation between each part and the GWF was calculated. The results are summarised in the succeeding paragraphs.

From the first part, the correlation coefficients between the tropospheric wind variability at different altitudes, and the GWF had values between -0.1300 and -0.2865, significantly correlated above the 99% confidence level. However, when a high pass Butterworth filter was used to remove seasonal trends, the correlation coefficients dropped and became insignificant. Since the correlation coefficients were small to begin with, the concluding mark was that the relation to the GWF was rather weak. And that the correlation that first was seen was mainly an effect from the seasonal variability in both the tropospheric winds and the GWF.

In the second part, the GW activity or more specifically, the kinetic energy per unit mass in the lower stratosphere (15-22 km in altitude), was estimated from radiosonde data. A significant correlation coefficient with the GWF of -0.2958 was found. To account for seasonal trends a different method was used than in the previous part due to the lack of data from the radiosonde measurements, with 29% missing. Thus, the filter used before could not be applied here. This was solved by only looking at the summer months' worth of data. The result was that the correlation coefficient became small and insignificant. This indicated that the connection to the GWF was again highly based on seasonal variability.

As an additional consideration, a study between the tropospheric wind variability (at different altitudes) and the GW activity in the lower stratosphere was done. This revealed correlation coefficients between 0.3184 and 0.5008, significantly correlated above the 99% confidence level. Like above, when only looking at the summer months' worth of data, the correlation dropped and became insignificant. This showed that seasonal effects had a large impact on this connection as well.

In the third part, the GW filtering by the stratospheric wind profile, which was called the net zonal wind, was studied. A significant correlation coefficient of -0.6472 was discovered between this and the GWF. Comparable to the other parts, the correlation dropped and became insignificant when the high pass filter was applied. This illustrated again that it was the seasonality that mainly linked the atmosphere together.

Finally, to see how the strength of the GWs affected the GWF, their phase speed range, which was uniformly distributed around 0, was looked into. It was found that GWs with phase speeds within $\pm$ 46 m/s had the greatest effect on the GWF, with a significant correlation coefficient of 0.6932. When the same filter was applied to this data set, the correlation dropped and became insignificant. This illustrated once more the seasonal effect.

It is reasonable that the results from this analysis were mainly driven by the seasonal cycle. After all, both the troposphere and the stratosphere are highly governed by the seasons. Hence, the GW generation, the GW activity and the GW filtering are highly governed by the seasons. And this seasonal trend also impacts the MLT. When this factor was removed through filtering, the correlation coefficient should drop as was the case for all parts. Even though the high frequency variability in the GWF could not be explained in more detail, one thing is however important to emphasise. Namely, that the combination of the unfiltered GW phase speed range and the stratospheric filter slightly improved the correlation with the GWF. It went from explaining 42% of the variance when only considering the stratospheric filter (net zonal wind), to 48% when combining the stratospheric filter with the GW phase speed range. This is an interesting result as this approach indicates that weather and climate models could be improved by implementing a restriction on the GWs. To put it differently, GWs in a particular range, which is known to have the highest impacts in the MLT, could increase the accuracy in models compared to choose an arbitrary range. On the other hand, the results are somewhat surprising as section 2.3 would suggest a higher connection between the stratospheric filter and the GWs propagating to the MLT. However, not all mechanisms on GW generation and activity in the middle atmosphere are fully understood. There are, as mentioned in section 2.2, other dynamics influencing the GWs in the atmosphere that are still being researched and are not yet quantified (Fritts and Alexander, 2003). More research on all the dynamics affecting GW generation and activity is highly desirable to get a better understanding of GW behavior.

Further, it is also important to be aware of the limitations to this analysis, which is restricted to Trondheim in 2013. With this said, the results obtained could be argued to have more or less ruled out a relationship between GWs in the troposphere and stratosphere and the high frequency variability in the GWF measured by de Wit et al. (2014). Therefore, outlooks to future studies would be to consider possible mechanisms happening in the MLT itself or above. This could be done by the use of satellite measurements or by ground based radars like the SKiYMET. It would also be beneficial to have longer time series to work with, both from the climate model and the radiosondes. Radiosonde data with better vertical resolution would also be desirable. With more data available to perform the analysis it would be possible to compare the year-to-year variability as well. Moreover, 2013 might not have been the best year to perform a study, since a major SSW took place in January. This altered the atmosphere for a short period of time and its impacts could be felt beyond the MLT (e.g. de Wit et al., (2014); Holton (1983)).

To sum up, this thesis, despite its spatial and temporal limits, has come to the conclusion that GW generation and activity in the troposphere and stratosphere cannot explain the high frequencies in the GWF. At least not with today's knowledge about GW dynamics and effects in the atmosphere. Suggestions to future work are to research GW dynamics in the middle atmosphere in greater detail, using longer time series and to look into possible mechanisms affecting the GW generation and breaking in or above the MLT.

Bibliography

[1] Andrews, D. G. (2005) *An Introduction to Atmospheric Physics*, 3rd printing, Cambridge University Press

[2] Coy, L., Pawson, S. (2013) *GEOS-5 Analysis and Forecasts of the Major Stratospheric Sudden Warming of January 2013,* Global modeling and assimilation office, NASA
Available at: http://gmao.gsfc.nasa.gov/researchhighlights/SSW/ [March 20 2015]

[3] de Wit, R.J. (2015) *Quantifying the influence of the stratosphere on the mesosphere and lower thermosphere,* doctoral thesis, NTNU

[4] de Wit, R.J., Hibbins, R.E., Espy, P.J. (2014) *The seasonal cycle of gravity wave momentum flux and forcing in the high latitude northern hemisphere mesopause region,* Journal of atmospheric and solar-terrestrial physics
Available at: http://www.sciencedirect.com/science/article/pii/S1364682614002296 [February 21 2015]

[5] de Wit, R.J., Hibbins, R.E., Espy, P.J., Orsolini, Y.J., Limpasuvan, V., Kinnison, D.E. (2014) *Observations of gravity wave forcing of the mesopause region during the January 2013 major Sudden Stratospheric Warming,* Geophysical research letters, 41
Available at: http://onlinelibrary.wiley.com/doi/10.1002/2014GL060501/epdf [March 23 2015]

[6] de Wit, R.J., Hibbins, R.E., Espy, P.J., Hennum, E.A. (2013) *Coupling in the middle atmosphere related to the 2013 major Sudden Stratospheric Warming,* Annales geophysicae

[7] Department of Atmospheric Science, University of Wyoming (2013) *Upper air data - sounding*
Available at: http://weather.uwyo.edu/upperair/sounding.html [March 27 2015]

[8] Earth Data, NASA (2014) *MDISC Data Subset*
Available at:
http://disc.sci.gsfc.nasa.gov/daac-bin/FTPSubset.pl?LOOKUPID_List=MAI6NPANA
[February 6 2015]

[9] Earth Observatory, NASA (2014) *Measuring Earth's albedo*
Available at: http://earthobservatory.nasa.gov/IOTD/view.php?id=84499 [February 19 2015]

[10] Espy, P. J. (2015) *FY3201 Atmospheric Physics and Climate Change,* physics course given at NTNU, Trondheim

[11] Fritts, D. and Alexander, M. (2003) *Gravity wave dynamics and effects in the middle atmosphere*, Reviews of geophysics, 41(1), 1003, doi:10.1029/2001RG000106
Avaiable at: http://www.researchgate.net/profile/David_Fritts/publication/234038632_Gravity_wave_dynamics_and_effects_in_the_middle_atmosphere/links/00463536b46ca3ff4a000000.pdf [May 13 2015]

[12] Global Modeling and Assimilation Office (2012) *MERRA: Modern-era retrospective analysis for research and applications*
Available at: http://gmao.gsfc.nasa.gov/research/merra/intro.php [February 9 2015]

[13] Hibbins, R. E. (2015) personal communication

[14] Hocking, W. K. (2001) *Buoyancy (gravity) waves in the atmosphere*
Available at: http://www.physics.uwo.ca/∼whocking/p103/grav_wav.html [February 20 2015]

[15] Hocking, W. K., Fuller, B. and Vandepeer, B. (2001) *Real-time determination of meteor-related parameters utilizing modern digital technology,* Journal of atmospheric and solar-terrestrial physics 63 (2001) 155-169
Available at: http://www.sciencedirect.com/science/article/pii/S1364682600001383 [March 25 2013]

[16] Hocking, W. K. (2005) *A new approach to momentum flux determinations using SKiYMET meteor radars,* Annales geophysicae, 23, 2433-2439, doi:10.5194/angeo-23-2433-2005
Available at: http://www.ann-geophys.net/23/2433/2005/angeo-23-2433-2005.pdf [March 27 2015]

[17] Hoffmann, P., Jacobi, Ch. (2012) *Simulation of sudden stratospheric warmings with the Middle and Upper Atmosphere Model,* University of Leipzig
Available at:
http://www.uni-leipzig.de/∼jacobi/docs/Hoffmann_2012_LIM_SSW_Model.pdf
[March 23 2015]

[18] Holton, J. R. (2004) *An introduction to dynamic meteorology,* 4th edt., Elsevier Inc.
Available at: http://www.dca.ufcg.edu.br/DCA_download/An%20Introduction%20to%20Dynamic%20Meteorology.pdf [March 20 2015]

[19] Holton, J. R. (1983) *The influence of gravity wave breaking on the general circulation of the middle atmosphere,* Journal of atmospheric science, vol.40, pages 2497-2507
Available at: http://www-k12.atmos.washington.edu/∼gcg/JR_site/papers/1983_4.pdf [March 19 2015]

[20] IPCC Fifth Assessment Report (2014) *Annex III: Glossary*
Available at:
https://www.ipcc.ch/pdf/assessment-report/ar5/wg1/WG1AR5_AnnexIII_FINAL.pdf
[February 18 2015]

[21] Lindzen, R. S. (1981) *Turbulence and stress owing to gravity wave and tidal breakdown,* Journal of geophysical research, vol. 86, pages 9707-9714
Available at: http://eaps.mit.edu/faculty/lindzen/97trbs∼1.pdf [March 19 2015]

[22] Lucchesi, R. (2012) *File specification for MERRA products,* GMAO office note no. 1 (version 2.3)
Available at:
http://gmao.gsfc.nasa.gov/products/documents/MERRA_File_Specification.pdf [February 21 2015]

[23] Ma, Q. (1998) *Greenhouse Gases: Refining the Role of Carbon Dioxide*
Available at: http://www.giss.nasa.gov/research/briefs/ma_01/ [February 18 2015]

[24] Moffat-Griffin, T., R. E. Hibbins, M. J. Jarvis, and S. R. Colwell (2011) *Seasonal variations of gravity wave activity in the lower stratosphere over an Antarctic Peninsula station*, Journal of geophysical research, 116, D14111, doi:10.1029/2010JD015349.

[25] Mukhtarov P., Pancheva, D, Andonov, B., Mitchell, N.J., Merzlyakov, E., Singer, W., Hocking, W., Meek, C., Manson, A. and Murayama, Y. (2007) *Large-Scale Thermodynamics of the Stratosphere and Mesosphere during the Major Stratospheric Warming in 2003/2004,* Journal of atmospheric and solar-terrestrial physics, 69 (17-18), pp. 2338-2354
Available at:
http://opus.bath.ac.uk/414/1/Pancheva_Jnl_Atmos_Sol-Terr_Phys_2007.pdf [March 24 2015]

[26] Norwegian Meteorological Institute (2009) *Radiosonder*
Available at: https://metlex.met.no/wiki/Radiosonder [April 24 2015]

[27] Plane, J. M. C. (2003) *Atmospheric chemistry of meteoric metals,* Chemical reviews, 103 (12), 4963 - 4984.
Available at: http://pubs.acs.org/doi/pdf/10.1021/cr0205309 [February 19 2015]

[28] Ramaswamy, V. (2006) *Why do temperatures vary vertically (from the surface to the stratosphere) and what do we understand about why they might vary and change over time?* U.S. climate change science program, synthesis and assessment product 1.1
Available at: http://www.gfdl.noaa.gov/bibliography/related_files/vr0603.pdf [March 22 2015]

[29] Rienecker, M.M., Suarez, M.J., Todling, R., Bacmeister, J., Takacs, L., Liu, H.-C., Gu, W., Sienkiewicz, M., Koster, R.D., Gelaro, R., Stajner, I. and Nielsen, E. (2008) *The GEOS-5 Data Assimilation System - Documentation of Versions 5.0.1, 5.1.0, and 5.2.0,* Technical report series on global modeling and data assimilation, vol. 27
Available at: http://gmao.gsfc.nasa.gov/pubs/docs/Rienecker369.pdf [May 7 2015]

[30] Siikamäki, R. (2004) *Supporting synoptic observations in Norway,* Vaisala News no. 164, page 10
Available at: http://www.vaisala.com/Vaisala%20Documents/Vaisala%20News%20Articles/VN164/VN164_AllPages.pdf [May 2 2015]

[31] Singer, W., von Zahn, U., Weiß, J. (2004) *Diurnal and annual variations of meteor rates at the Arctic circle,* Atmospheric chemistry and physics, vol. 4, 1355-1363
Available at: http://www.atmos-chem-phys.net/4/1355/2004/acp-4-1355-2004.pdf [March 19 2015]

[32] Stray, N. H. (2015) personal communication

[33] Stuver, A.L (2013) *Q: What's the Difference Between a "Gravitational Wave" and a "Gravity Wave?"*
Available at: http://stuver.blogspot.no/2013/01/q-whats-difference-between.html [March 13 2015]

[34] Vincent, R. A. (2009) *Gravity wave coupling from below: A review*
Available at:
http://www.terrapub.co.jp/onlineproceedings/ste/CAWSES2007/pdf/CAWSES_279.pdf [February 22 2015]

[35] Vincent, R. A., and M. J. Alexander (2000) *Gravity waves in the tropical lower stratosphere: An observational study of seasonal and interannual variability*, Journal of geophysical research, 105, 17,971–17,982
Available at: http://onlinelibrary.wiley.com/doi/10.1029/2000JD900196/pdf [April 16 2015]

[36] Whiteway, J. A. and Carswell, A. I. (1994) *Rayleigh Lidar Observations of Thermal Structure and Gravity Wave Activity in the High Arctic during a Stratospheric Warming,* Journal of the atmospheric science, 51, 3122-3136
Available at:
http://journals.ametsoc.org/doi/pdf/10.1175/1520-0469%281994%29051%3C3122%3ARLOOTS%3E2.0.CO%3B2 [March 24 2015]

[37] **Figure**; Earth Observatory, NASA (2004) *Gravity Waves Ripple over Marine Stratocumulus Clouds*
Available at: http://earthobservatory.nasa.gov/IOTD/view.php?id=4117 [March 29 2015]

[38] **Figure**; Gibson, S. (2014) *Gravity waves over New hampshire/Vermont*
Available at:
http://blog.weatherflow.com/gravity-waves-over-new-hampshirevermont/ [February 21 2015]

[39] **Figure**; Hithcock, M. D. (2005) Information Service, Atmospheric layers,
Available at: http://www.geogrify.net/GEO1/Lectures/IntroPlanetEarth/FourSpheres.html [February 18 2015]

[40] **Figure**; Oklahoma Climatological Survey (1997),
Available at: http://okfirst.mesonet.org/train/meteorology/EnergyBudget2.html [February 18 2015]

Appendix A: Matlab code

Matlab code used for the analysis.

Loading the MERRA data

```
%Load each file, specifying latitude and longitude
%Divide into two parts Jan-Sep (month 1-9) and Oct-Dec(month 10-12)

%Make vector monthDay with the right amount of days in each month
monthDay=zeros(365,2);
for i=1:31 %Jan, Mar, May, July, Aug, Oct, Dec
    monthDay(i,1)=1;
    monthDay(i,2)=i;
    monthDay(i+59,1)=3;
    monthDay(i+59,2)=i;
    monthDay(i+120,1)=5;
    monthDay(i+120,2)=i;
    monthDay(i+181,1)=7;
    monthDay(i+181,2)=i;
    monthDay(i+212,1)=8;
    monthDay(i+212,2)=i;
    monthDay(i+273,1)=10;
    monthDay(i+273,2)=i;
    monthDay(i+334,1)=12;
    monthDay(i+334,2)=i;
end

for i=1:30 %Feb, Apr, June, Sept, Nov
    monthDay(i+31,1)=2;
    monthDay(i+31,2)=i;
    monthDay(i+90,1)=4;
    monthDay(i+90,2)=i;
    monthDay(i+151,1)=6;
    monthDay(i+151,2)=i;
    monthDay(i+243,1)=9;
    monthDay(i+243,2)=i;
    monthDay(i+304,1)=11;
    monthDay(i+304,2)=i;
end
%Correcting for Feb
```

```
monthDay(60,2)=1; monthDay(61,2)=2; monthDay(62,2)=3;
monthDay(60,1)=3; monthDay(61,1)=3; monthDay(62,1)=3;

%Load the files day by day and put them into a struct AB,
%set wind speed>200 to NaN,
%find min/max value and difference between min/max, all over Trondheim
dailyMaxU=zeros(365,1); dailyMinU=zeros(365,1); DIFF=zeros(365,1);
for numDays=1:273 %Jan through Sep
    if monthDay(numDays,2)<10 %Jan-Sep in file
        load(...
          strcat('C:\Users\Hanne\Dropbox\NTNU\MASTER\Nv\MERRA20130',...
          num2str(monthDay(numDays,1)),'0',...
          num2str(monthDay(numDays,2)),'.mat'));
    else %Oct-Dec in file
         load(...
          strcat('C:\Users\Hanne\Dropbox\NTNU\MASTER\Nv\MERRA20130',...
          num2str(monthDay(numDays,1)),...
          num2str(monthDay(numDays,2)),'.mat'));
    end

    datevec(MERRA.datenum) %shows the date
    AB(numDays).date=MERRA.datenum; %date vector

        for long=1:34
            for lat=1:27
                for alt=1:72
                %Putting unrealistic wind speed values to NaN
                AB(numDays).u(long,lat,alt)=MERRA.u(long,lat,alt);
                AB(numDays).v(long,lat,alt)=MERRA.v(long,lat,alt);
                    if AB(numDays).u(long,lat,alt)>200
                       AB(numDays).u(long,lat,alt)=NaN;
                    end
                end

               %Put maxU and minU for each long. and lat. into this
               AB(numDays).uMax(lat,long)=...
                    max(AB(numDays).u(long,lat,:));
               AB(numDays).uMin(lat,long)=...
                    min(AB(numDays).u(long,lat,:));
            end
        end

        %-------------------------Just over TRD-------------------------------
        for Tlong=1:2
            for Tlat=1:2
               %Finding max for the coordinates closest to Trondheim
               %(4 coordinates=4 values)
```

```
                AB(numDays).TuMax(Tlat,Tlong)=...
                    max(AB(numDays).uMax(Tlong+9,Tlat+12,:));
                AB(numDays).TuMin(Tlat,Tlong)=...
                    min(AB(numDays).uMin(Tlong+9,Tlat+12,:));
            end
        end
        %Max/min value and difference
        dailyMaxU(numDays)=max(AB(numDays).TuMax(:));
        dailyMinU(numDays)=min(AB(numDays).TuMin(:));
        DIFF(numDays)=(dailyMaxU(numDays)+dailyMinU(numDays))/2;
end

for numDays=274:365 %Oct through Dec
    if monthDay(numDays,2)<10
        load(...
          strcat('C:\Users\Hanne\Dropbox\NTNU\MASTER\Nv\MERRA2013',...
          num2str(monthDay(numDays,1)),'0',...
          num2str(monthDay(numDays,2)),'.mat'));
    else
        load(...
          strcat('C:\Users\Hanne\Dropbox\NTNU\MASTER\Nv\MERRA2013',...
          num2str(monthDay(numDays,1)),...
          num2str(monthDay(numDays,2)),'.mat'));
    end

    datevec(MERRA.datenum) %shows the date
    AB(numDays).date=MERRA.datenum; %date vector

       for long=1:34
            for lat=1:27
                for alt=1:72
                %Putting unrealistic winds speed values to NaN
                AB(numDays).u(long,lat,alt)=MERRA.u(long,lat,alt);
                AB(numDays).v(long,lat,alt)=MERRA.v(long,lat,alt);
                    if AB(numDays).u(long,lat,alt)>200
                       AB(numDays).u(long,lat,alt)=NaN;
                    end
                end

               %Putt maxU and minU for each long. and lat. into this
               AB(numDays).uMax(lat,long)=...
                    max(AB(numDays).u(long,lat,:));
               AB(numDays).uMin(lat,long)=...
                    min(AB(numDays).u(long,lat,:));
            end
       end
```

```
        %-------------------------Just over TRD-------------------------
        for Tlong=1:2
            for Tlat=1:2
               %Finding max for the coordinates closest to Trondheim
                %(4 coordinates=4 values)
                AB(numDays).TuMax(Tlat,Tlong)=...
                    max(AB(numDays).uMax(Tlong+9,Tlat+12,:));
                AB(numDays).TuMin(Tlat,Tlong)=...
                    min(AB(numDays).uMin(Tlong+9,Tlat+12,:));
            end
        end
        %Max/min value and difference
        dailyMaxU(numDays)=max(AB(numDays).TuMax(:));
        dailyMinU(numDays)=min(AB(numDays).TuMin(:));
        DIFF(numDays)=(dailyMaxU(numDays)+dailyMinU(numDays))/2;
end
```

High pass filter to remove seasonal trends

```
%In Matlab write
fdatool

%Responsetype: highpass
%Design method: IIR Butterworth
%Filter order: minimum order
%Options: match exactly passband
%Frequency specifications: units=Hz, Fs=1, Fstop=1/90, Fpass=1/50
%(A sample frequency of 1 per day makes Hz in cycles per day)
%Magnitude specifications: units=dB, Astop=20dB, Apass=1

%Click on "Design filter"

%Click on "Edit": Convert to a single section
%Click on "File": Export; Workspace; Coefficients; Num; Den; Export

%To use this filter:
Y=filtfilt(Num, Den, x) %where x is the data series you want to filter
```

Part 1: Tropospheric wind variability

```
%Taking out u and v values over TRD at lvl 17 = 703hPa, into uTopo/vTopo
%Calculate wTopo (net winds speed) and correlate with GWF,
%with and without filter
uTopo=zeros(365,1); vTopo=zeros(365,1); wTopo=zeros(365,1);
corrU=zeros(30,1); corrW=zeros(30,1); pval=zeros(30,1);
%Filter
```

```
FcorrW=zeros(30,1); Fpval=zeros(30,1);
Y=filtfilt(Num, Den, gwf.F);
for hPa=1:30 %altitude range
    for day=1:365
     for j=1:2 %latitude
        for k=1:2 %longitude
           AB(day).uTopo1(j,k)=AB(day).u(9+j,12+k,hPa);
           AB(day).vTopo1(j,k)=AB(day).v(9+j,12+k,hPa);
        end
     end
     %Averaging over the four points
     uTopo(day)=mean(AB(day).uTopo1(:));
     vTopo(day)=mean(AB(day).vTopo1(:));
     %Vector sum of u and v
     wTopo(day)=sqrt(uTopo(day)^2+vTopo(day)^2);
    end

 CorrwTopo=wTopo(6:360); %no filter
 FCorrwTopo=filtfilt(Num, Den, wTopo(6:360)); %FILTER

 [RHO, PVAL]=corr(CorrwTopo(:), gwf.F(:)); %no filter
 [fRHO, fPVAL]=corr(FCorrwTopo(:), Y(:)); %FILTER

 corrW(hPa)=RHO; pval(hPa)=PVAL; %no filter
 FcorrW(hPa)=fRHO; Fpval(hPa)=fPVAL; %FILTER
end
```

Part 2: GW activity in the lower stratosphere

```
%Part 3, read in the radiosonde data
fileID = fopen('test.txt');

%Just reading the altitude, temperature and wind speed from the file
A = textscan(fileID,'%*d %f32 %f32 %*d %*d %*d %*d %f32 %*d %*d %*d');
alt=A{1}; temp=A{2}; knot=A{3};
fclose(fileID);

lenFile=length(alt);

%----------------Plot the wind between 15-22km----------------------------
countPol=0;
for exe=1:lenFile
    %taking out the values in this range
 if alt(exe)>15000 && alt(exe)<22000
    %number of data points within this range
    countPol=countPol+1;
    %take out the wind speed within this range
```

```
    knotPolTest(exe)=knot(exe);
 end
end

lengthKnot=length(knotPolTest);
start=lengthKnot-countPol+1;%the first altitude above 15km
for ixe=1:countPol
    %new vector containg wind speed
    knotPol(ixe)=knotPolTest(start-1+ixe);
end

%Plot of wind speed vs. altitude
figure
plot(knotPol(:),alt(start:lengthKnot),'-o')
xlabel('Wind speed [knots]'); ylabel('Altitude [m]');

%-----------------Polynomial fit-----------------------------------------
t=alt(start:lengthKnot); %Altitude vector, independent variabel
y=knotPol(:).*0.5144; %Wind speed converted to M/S, dependent variabel
p=polyfit(t,y,2); %polyfit command
y2=polyval(p,t); %polyfit evaluated at each altitude

%Plot of the original data and the polynomial fit
figure
plot(t,y,'-o',t,y2,':')
ylabel('Wind speed [m/s]'); xlabel('Altitude [m]');

%-----------------Finding the residual evaluated at the original data---
res=y-y2;

%Plot of the residuals
figure
plot(t,res,'-o')
line([14000 23000], [0 0], 'LineStyle',':','color', 'k');
ylabel('Residual [m/s]'); xlabel('Altitude [m]');

%-----------------KE/kg=var/2--------------------------------------------
KE=var(res)/2;

%-----------------KE/kg for all months-----------------------------------
Jan00=[4.0531, NaN, 2.6962, 3.8934, 2.7764, 2.2328, 2.3151, NaN,...
    2.0170, 1.7730, 1.4983, 3.3854, 4.4438, NaN, 2.1807, 1.6293,...
    2.1238, NaN, 4.3356, 2.5044, NaN, NaN, NaN, 13.4445, 6.8460, 6.0337];
Jan12=[4.9198, 7.0228, 5.576, NaN, 5.0199, 1.9922, NaN, NaN, 3.996,...
    2.4317, 3.8112, 3.0778, 2.2704, 4.8807, 3.0518, 1.3697, 2.5001,...
    NaN, 5.4861, NaN, NaN, NaN, NaN, 23.0172, 3.6273, NaN];
```

```
Feb00=[NaN, 6.5007, 3.7919, 7.0882, 4.2449, 3.1203, 1.6168, 0.3607,...
    1.7685, NaN, 3.4297, 2.9007, 0.9834, 2.1652, 0.5763, 0.7753,...
    1.4473, 1.7440, 1.9290, NaN, 2.7814, 4.9098, 4.6075, 3.2824,...
    6.2440, 3.6717, 12.4740, NaN];
Feb12=[5.0370, 2.5860, NaN, 7.5529, NaN, NaN, NaN, 1.1967, 0.4825,...
    2.1706, 2.4904, 1.9774, 1.6796, NaN, 1.3460, 1.2943, 2.2540,...
    2.0151, 2.9455, 1.0979, 2.4143, 3.1841, 4.7577, 4.9277, NaN,...
    3.3469, 8.1639, 7.8331];

Mar00=[NaN, 5.5275, NaN, NaN, 5.7141, NaN, NaN, NaN, NaN, NaN,...
    1.0000, 3.0007, NaN, NaN, 2.4182, 2.1193, NaN, 2.8914, 3.5640,...
    1.5569, NaN, NaN, NaN, NaN, NaN, 2.2690, NaN, 2.1007, 1.5594,...
    1.9304, NaN];
Mar12=[6.1330, NaN, NaN, NaN, NaN, NaN, NaN, 4.5605, NaN, 1.5821,...
    NaN, 7.5983, NaN, 2.5823, 3.9235, 1.5789, 2.4021, NaN, 2.6020,...
    3.2013, 1.9128, 3.3810, 2.3199, NaN, NaN, 1.6730, 1.7500, NaN,...
    NaN, NaN, 1.9611];

Apr00=[NaN, 2.6882, 2.1461, 1.8628, NaN, NaN, NaN, NaN, NaN, NaN,...
    2.3497, NaN, NaN, 3.8215, 8.6091, 10.9675, 4.5563, NaN, NaN,...
    NaN, 4.3322, 3.3345, 11.6058, 6.5302, NaN, NaN, NaN, NaN,...
    NaN, 2.4273];
Apr12=[NaN, 2.5210, 3.3015, 3.4336, 3.6660, NaN, NaN, 2.0607,...
    NaN, NaN, NaN, NaN, 2.3993, 4.1952, 4.8235, 1.6195, 6.5708,...
    6.3961, 8.0573,8.5708, 3.0611, 8.0768, 5.9623, 25.1747,...
    NaN, NaN, NaN, NaN, NaN, 3.2590];

May00=[5.2945, 5.5893, NaN, 2.7679, 4.3590, 2.4277, 5.3599, 4.5328,...
    2.8787, 1.3485, 3.2978, 1.6515, 2.9715, 1.2963, 2.1181, NaN, NaN,...
    NaN, NaN, NaN, 3.2482, NaN, 2.1240, 2.3682, NaN, 2.0324, 1.4977,...
    2.5157, 0.9730, 5.1417, 2.2369];
May12=[7.5477, 3.5729, 3.5911, 2.3758, NaN, 2.0325, 2.7061, 3.7709,...
    NaN, 2.8850, 3.0439, 2.2688, 1.7816, 2.7375, 2.9661, NaN, NaN,...
    NaN, NaN, NaN, 1.8147, 1.5124, NaN, NaN, NaN, 2.0111, 2.1061,...
    NaN, 4.2776, NaN, NaN];

Jun00=[NaN, NaN, NaN, NaN, 2.3833, NaN, 1.2192, 2.4626, 1.3206,...
    1.1494, 1.8122, 2.6870, 2.9719, 1.7922, 2.3427, 0.4098,...
    0.8970, 1.1633, 1.6523, NaN, 2.2115, 1.5965, 3.6978, 2.4176,...
    2.3540, 2.0539, 1.8161, 1.3819, 3.1071, 2.5257];
Jun12=[NaN, NaN, 1.8322, 0.8535, NaN, 1.0886, NaN, 1.3609, NaN,...
    0.3673, 1.4507, 2.4788, NaN, 1.7752, 1.1847, NaN, NaN,...
    2.2603, 1.8809, 3.0264, 3.0951, 0.9002, 3.4479, 4.0218, 1.7709,...
    1.8861, 2.6496, 1.2837, NaN, 2.8977];

Jul00=[1.8976, 2.1341, NaN, 1.2433, 1.1508, 1.0836, 1.6257, 2.7568,...
    1.9359, 1.3398, NaN, 1.8230, 2.1127, 1.8585, 3.1288, 3.1424,...
```

```
    1.2133, 2.1610, 2.3897, 2.6323, 2.3839, 0.9801, 2.2090, 0.8182,...
    1.1730, NaN, 1.8531, 1.5200, 3.0455, 4.2952, 3.3680];
Jul12=[2.7893, 1.5817, 2.0296, 1.1288, 2.5174, 2.0074, 1.7739,...
    2.3060, 1.3416, 1.8757, NaN, 2.5288, 0.8307, 2.3336, 1.1201,...
    1.6780, 1.6565, 1.8195, 2.2989, 4.3042, 3.1280, 1.0162, 1.9766,...
    1.1216, 3.4275, 2.5078, 1.1874, NaN, 2.6799, 3.1865, 2.5948];

Aug00=[1.6009, 1.6395, 2.3138, 3.4231, 4.1047, 2.2105, 1.8435,...
    2.4111, 1.6416, NaN, NaN, 1.2336, 0.5859, 1.6795, 0.5078,...
    1.5510, 0.9841, 1.7583, 2.9634, 3.5903, 3.9780, 3.6405, NaN,...
    2.7329, 1.6099, 2.7334, 0.8132, 1.9111, 2.0739, 3.5473, 2.1945];
Aug12=[2.1922, 1.7981, 5.1594, 3.7281, 1.8002, 2.1059, 2.5819,...
    1.7329, 2.2948, NaN, NaN, 0.8262, 0.5778, 0.6591, 1.2149,...
    3.0118, 1.7076, 1.2861, 1.6247, 2.6499, 3.2264, 3.3617, 0.9701,...
    2.0608, 0.3180, 1.8267, 2.2624, 1.9606, 2.3740, 3.2902, 1.1653];

Sep00=[2.8404, 4.8738, 3.6533, 1.8892, 3.3006, 3.2353, 2.0661, 2.0304,...
    3.0209, 1.6380, 1.2484, 1.1349, 1.3829, 0.8462, 2.0427, 1.8227,...
    1.9408, 1.8085, 2.8202, 2.4690, 0.4737, NaN, NaN, 5.8808, 3.6175,...
    1.6809, 1.1985, 2.3622, 1.1424, 1.8175];
Sep12=[2.5764, 2.4595, 2.8208, 3.2070, 3.0178, 2.2418, 2.7352,...
    3.0490, 2.7125, 2.7489, 0.8763, 1.8911, 0.4116, 0.8248, 3.1830,...
    2.0755, 2.5207, 3.1517, 1.9531, NaN, NaN, NaN, 8.8697, NaN,...
    2.7602, 0.9300, 1.2977, 0.7232, 2.0758, 1.6933];

Oct00=[3.1884, 1.2333, NaN, 0.8865, 1.5033, 2.9805, 8.4282, 4.3646,...
    2.4537, 4.4988, 6.4583, 5.0812, 2.8207, 4.5500, 4.0772, NaN, NaN,...
    3.2769, 3.6995, 2.6178, 1.3372, 1.5327, 3.0007, 0.5730, 5.4956,...
    2.1602, 5.2006, 7.0730, 1.2412, 5.6499, 6.5869];
Oct12=[1.6522, 2.0375, 1.8837, 0.8449, NaN, NaN, 6.4585, 3.0054,...
    3.6513, 2.8010, 5.6916, 3.6074, 3.0174, 2.7290, 2.1466,...
    1.0272, 5.1818, 3.2661, 2.3062, 0.9006, 0.6427, 2.6290, 3.8092,...
    1.6576, 10.3361, 9.2340, 7.2588, 5.5540, NaN, 2.3402, 10.4048];

Nov00=[15.1676, 8.6739, NaN, 2.0834, 1.8264, 0.9144, 2.1939, 4.4623,...
    8.1843, 4.1836, 6.9534, 12.1856, 17.7101, 7.9472, 3.3398, NaN,...
    19.3779, 2.1953, NaN, NaN, 2.8710, NaN, 4.7498, 29.9422, NaN,...
    20.6013, NaN, NaN, 3.4205, 14.9304];
Nov12=[13.7832, 12.5276, NaN, 1.1081, 2.9108, NaN, 3.3503, 3.1190,...
    4.8242, 7.5958, 5.0935, 11.6145, 13.6205, NaN, 5.6040, 8.9754,...
    16.3493, NaN, NaN, 7.7779, 5.9166, 2.8013, 6.8131, 6.9138,...
    15.6255, NaN, 14.8738, 12.4130, NaN, NaN];

Dec00=[11.8034, NaN, NaN, NaN, NaN, NaN, NaN, NaN, NaN, NaN, NaN, NaN,...
    NaN, NaN, NaN, NaN, NaN, NaN, NaN, NaN, NaN, 4.8977, 9.0781, NaN,...
    NaN, NaN];
Dec12=[NaN, NaN, NaN, NaN, NaN, NaN, 2.7350, NaN, NaN, 9.2586, 4.7319,...
```

```
    6.4017, NaN, NaN, NaN, NaN, NaN, 5.2398, 5.7592, NaN, NaN, 3.1947,...
    NaN, NaN, NaN, NaN];

%Making vectors for 00Z launches and 12Z launches
year00=[Jan00, Feb00, Mar00, Apr00, May00, Jun00, Jul00, Aug00,...
    Sep00, Oct00, Nov00, Dec00];
year12=[Jan12, Feb12, Mar12, Apr12, May12, Jun12, Jul12, Aug12,...
    Sep12, Oct12, Nov12, Dec12];

%Averaging where possible
meanYear=zeros(1,355);
for i=1:355
    if isnan(year00(i))==1
       meanYear(i)=year12(i);
    elseif isnan(year12(i))==1
        meanYear(i)=year00(i);
    else
        meanYear(i)=(year00(i)+year12(i))./2;
    end
end
```

Part 3: GW filtering

```
%Finds the net GW number for each range and correlates with the GWF
netGW=zeros(365,1); Corr=zeros(200,1); pval=zeros(200,1);
negNum=0; posNum=0;
for range=1:200 %setting the range
    for day=1:365
        %Counting all the negative numbers (westward winds)
        for j=1:range
            if (-j)>=(-range)
                if(-j)<dailyMinU(day)||(-j)>dailyMaxU(day)
                negNum=negNum+1;
                end
            end
        end
        %Counting all the positive numbers (eastward wind)
        for j=1:range
            if j<=range
                if j>dailyMaxU(day)||j<dailyMinU(day)
                posNum=posNum+1;
                end
            end
        end
        %One netGW-value each day
        netGW(day)=(posNum-negNum);
        posNum=0; negNum=0;
```

```
    end
%Correlate net GW number with GWF for Jan 6-Dec 26 2013
[RHO, PVAL]=corr(netGW(6:360),gwf.F(:));
Corr(range)=RHO;
pval(range)=PVAL;
end
```

Appendix B: Additional figures

Some additional figures.

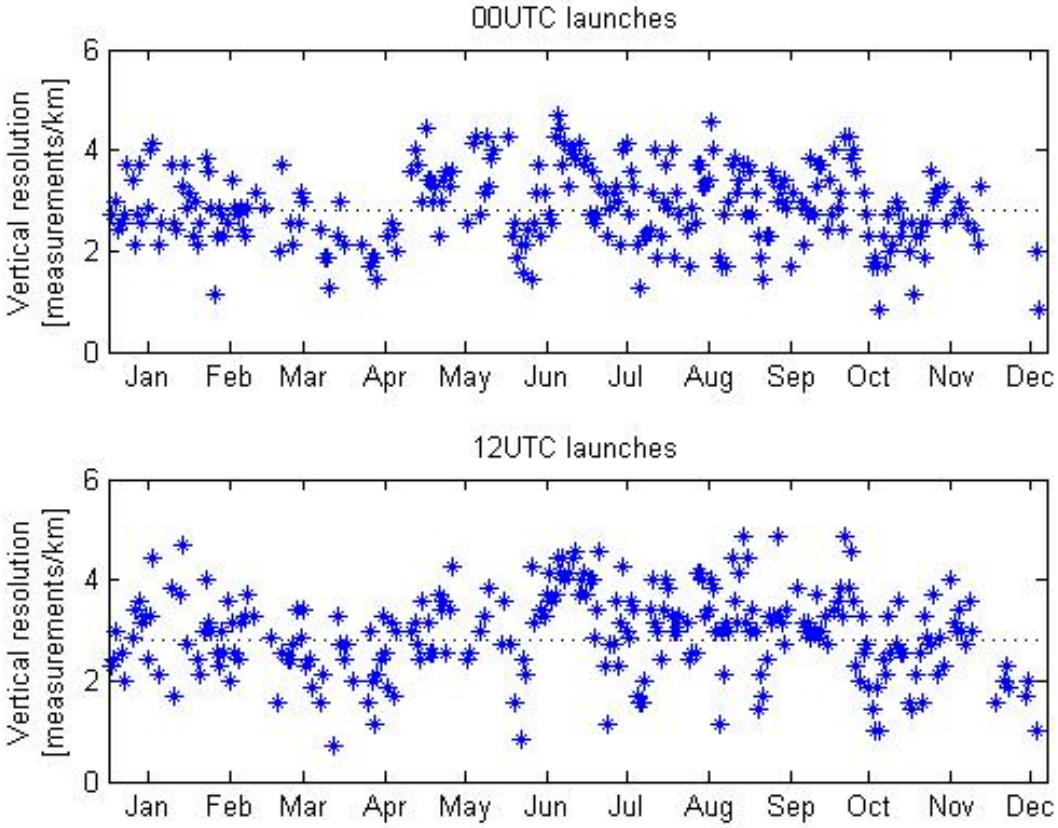

Figure 5.1: The vertical resolution, defined as the number of measurements per km taken by the ascending radiosondes, calculated on a daily basis for the 00UTC (top) and the 12UTC (bottom) launches in 2013.

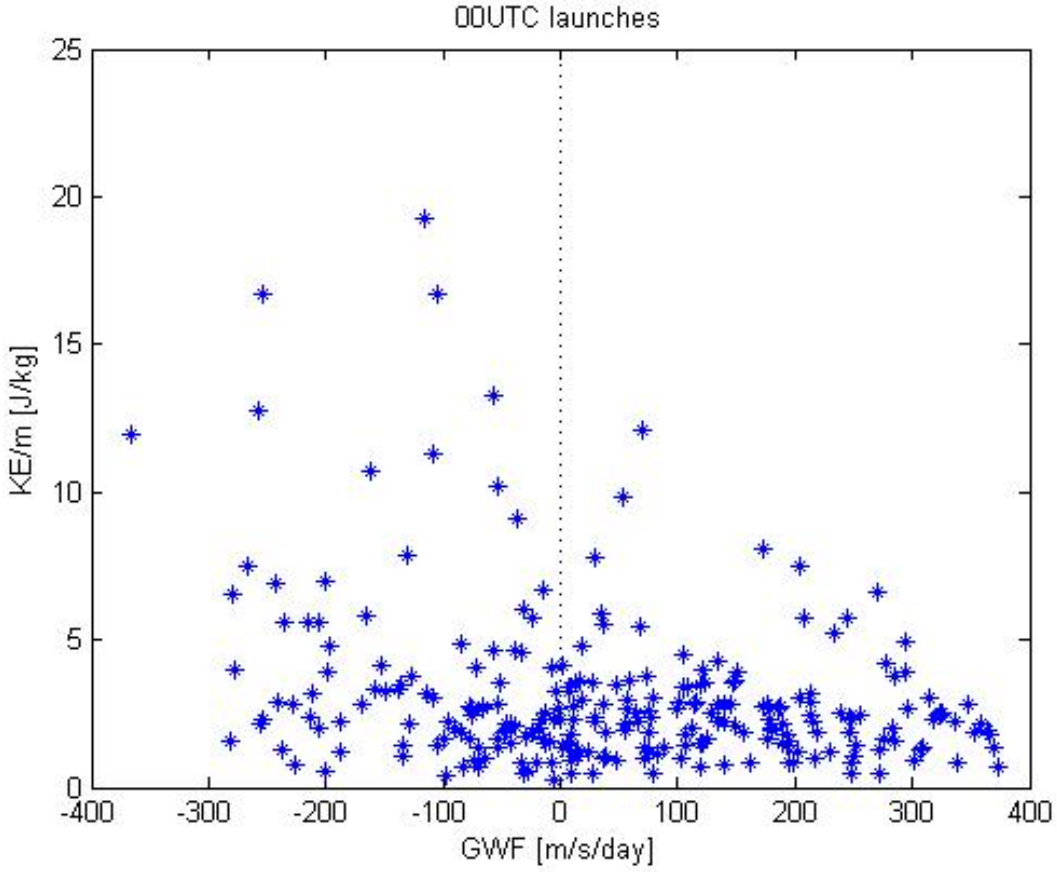

Figure 5.2: The GWF in the MLT versus the KE/m (GW activity) in the lower stratosphere measured by the radiosondes launched at 00UTC in 2013.

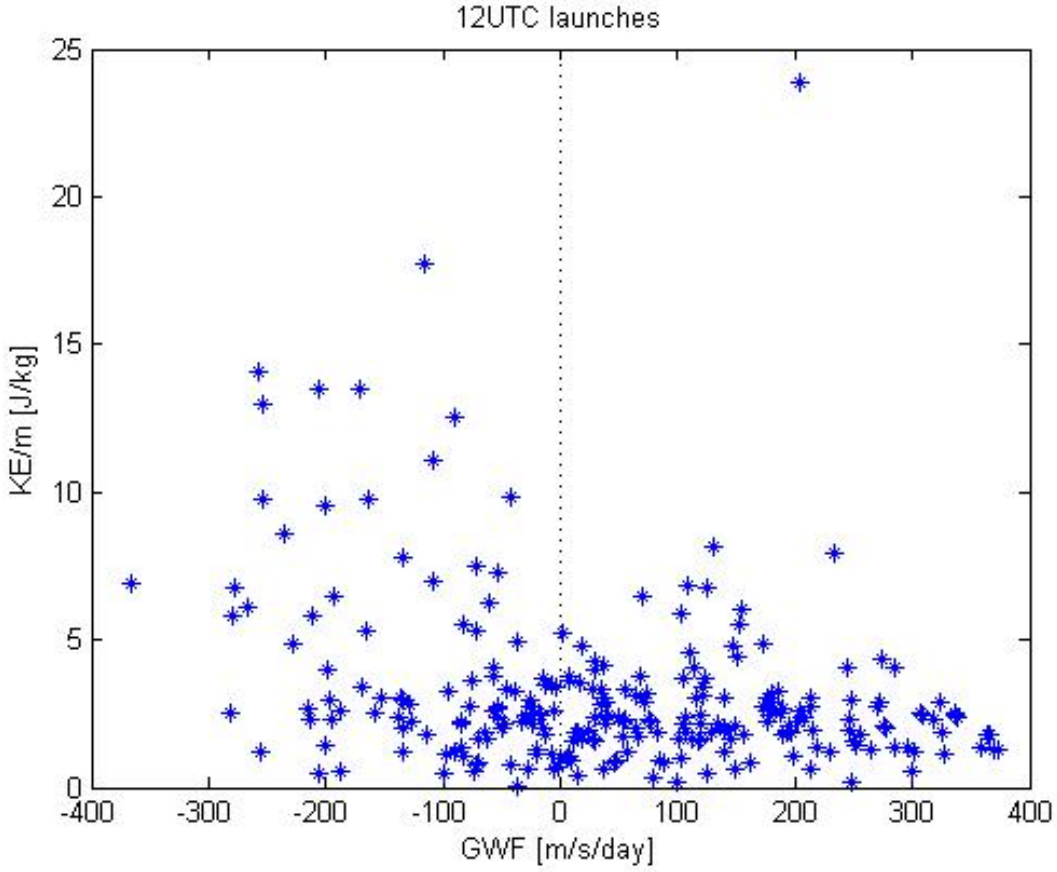

Figure 5.3: The GWF in the MLT versus the daily mean KE/m (GW activity) in the lower stratosphere measured by the radiosondes launched at 12UTC in 2013.